

Synthesis and Evaluation of Fluorine-18 Labeled 2-Phenylquinoxaline Derivatives as Potential Tau Imaging Agents

Kaixiang Zhou, Fan Yang, Yuying Li, Yimin Chen, Xiaojun Zhang, Jinming Zhang, Junfeng Wang, Jiawei Dai, Lisheng Cai,* and Mengchao Cui*

Cite This: *Mol. Pharmaceutics* 2021, 18, 1176–1195

Read Online

ACCESS |

Metrics & More

Article Recommendations

Supporting Information

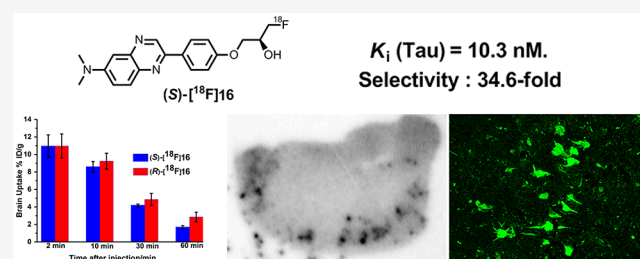
ABSTRACT: In this study, three pairs of optically pure ^{18}F -labeled 2-phenylquinoxaline derivatives were evaluated as Tau imaging agents for the diagnosis of Alzheimer's disease (AD). The chiral 2-fluoromethyl-1,2-ethylenediol side chain was attached to the 2-phenylquinoxaline backbone to increase hydrophilicity, thereby improving the binding affinity of the probe to tangles and their selectivity toward Tau tangles over β -amyloid plaques ($A\beta$). These probes displayed excellent fluorescent properties and high selectivity for tangles on brain sections from transgenic mice (rTg4510) and AD patients. Quantitative binding assays with AD homogenates showed that the probes (*R*)-5 and (*S*)-16 have a high affinity ($K_i = 4.1$ and 10.3 nM, respectively) and high selectivity (30.5-fold and 34.6-fold, respectively) for tangles over $A\beta$. The high affinity and selectivity of (*R*)-[^{18}F]5 and (*S*)-[^{18}F]16 for tangles were further confirmed with autoradiography on AD brain tissue *in vitro*. In addition, they displayed sufficient blood-brain barrier penetration (7.06% and 10.95% ID/g, respectively) and suitable brain kinetics ($\text{brain}_{2\text{ min}}/\text{brain}_{60\text{ min}} = 10.1, 6.5$ respectively) in normal mice. *Ex vivo* metabolism studies and micro-positron emission computed tomography (PET) revealed high brain biostability, good brain kinetic properties, and low nonspecific binding for (*S*)-[^{18}F]16. Together, these results demonstrate that (*R*)-[^{18}F]5 and (*S*)-[^{18}F]16 are promising PET probes for Tau tangles imaging.

KEYWORDS: Alzheimer's disease, Tau tangles, PET imaging, quinoxaline

INTRODUCTION

Alzheimer's disease (AD) is a type of neurodegenerative disorder and the main cause of dementia, resulting in serious threats to physical and mental health of the aged.^{1,2} The number of AD patients worldwide is predicted to exceed 106 million by the year 2050.³ However, the definitive etiopathogenesis of AD is still unclear. Post-mortem assessment of brain tissue from AD patients reveals two major pathological biomarkers: extracellular senile plaques consisting of β -amyloid ($A\beta$) peptides and intracellular neurofibrillary tangles (NFTs) consisting of hyperphosphorylated Tau proteins, as the gold standard biomarkers for the diagnosis of AD.⁴ Besides its complicated pathogenesis, the development of AD therapeutics is also impeded by the lack of diagnostic tools that may be used to stage and monitor the progression of the disease.⁵ It is therefore imperative to develop positron emission computed tomography (PET) imaging probes targeting the hallmarks of AD.⁶

$A\beta$ may not be a suitable biomarker for the monitoring of AD disease progression, especially in the later stage of the disease. Multiple PET probes have been developed and studied in a clinical setting to monitor AD progression. However, the correlation between the burden of $A\beta$ plaques and cognitive impairment in AD is not well-established, as some patients



with an $A\beta$ -positive PET scan displayed normal cognitive functions.^{7,8} As such, other hallmarks of the disease, downstream after the aggregation of $A\beta$ in brain, may be more appropriate to achieve diagnosis or staging of AD.⁹ For instance, the levels of misfolded Tau proteins in the brain correlate with the degree of neuronal degeneration and cognitive decline in AD.^{10–12} The Tau protein is a microtubule-associated protein naturally existing in axons that stabilize microtubules, regulate the plasticity of the cytoskeleton, and promote neurite outgrowth. The metabolic pathway of the Tau protein is controlled by hyperphosphorylation and dephosphorylation. In abnormal cases, the hyperphosphorylated Tau proteins accumulate as paired helical filaments, further leading to cytoskeletal dissociation and neurodeterioration.^{13,14} In addition, abnormal Tau aggregation is also associated with varieties of neurodegenerative disorder such as progressive supranuclear palsy, sporadic corticobasal

Received: November 1, 2020
Revised: December 27, 2020
Accepted: December 28, 2020
Published: January 21, 2021



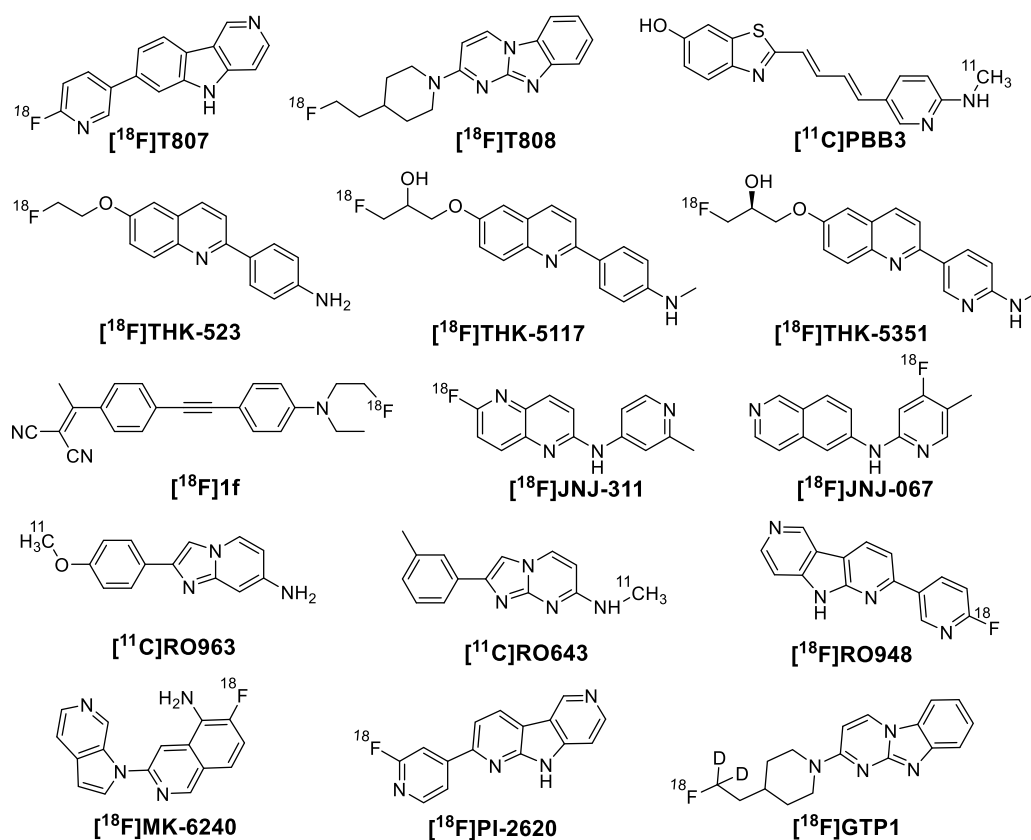


Figure 1. Chemical scaffolds evaluated as PET probes for Tau.

degeneration, Pick's disease, frontotemporal dementia, and Parkinsonism linked to chromosome 17.¹⁵ The quantitative evaluation of Tau level in the cerebrospinal fluid would advance the understanding of tauopathies, providing information on curative effects and, ultimately, accelerating drug discovery in antitau therapeutic trials.^{9,16,17} However, lumbar puncture is invasive, and the Tau level in the cerebrospinal fluid does not reflect the regional tissue distribution of Tau and its aggregates.¹⁸ Therefore, PET probes with specific binding with Tau aggregates would allow for the noninvasive visualization and subsequent quantification of Tau burdens in AD brains.

The first generation of PET Tau tracers, namely, [¹⁸F]T807 and [¹⁸F]T808, showed a high selectivity for Tau aggregates over A β plaques (25- and 27-fold, respectively, Figure 1). The probe [¹⁸F]T808 showed metabolic defluorination, while [¹⁸F]T807 was approved by the Food & Drug Administration (FDA) to image Tau pathology in patients being evaluated for AD. This significant progress gave a sign that these Tau tracers hold great promise for AD evaluation and diagnosis.^{19–24} THK derivatives with a 2-arylquinoline scaffold are another class of PET probe of Tau aggregates.^{25,26} The first in-human PET study of [¹⁸F]THK-5117 demonstrated that the PET images reflect the known NFTs distribution in an AD brain. However, this probe suffered from binding to subcortical white matter and unsuitable pharmacokinetics.^{27–29} A structural analogue, [¹⁸F]THK-5351, featuring a single (*S*)-enantiomer and pyridine ring, displayed improved pharmacokinetics and showed a high signal-to-noise ratio in PET images, when applied in AD patients.^{30,31} Another promising Tau probe, [¹¹C]PBB3, with two *trans* carbon–carbon double bonds, showed selective affinity for Tau aggregates in both in vitro and

human PET studies. However, the *E/Z* isomerization of the probe during radiochemical synthesis, even in the presence of room light, may be problematic and should not be ignored.^{32–34} The first-generation ligands have been deeply studied in human clinical trials but demonstrated varying degrees of off-target binding.

Subsequent to the optimization of binding properties and pharmacokinetics, second-generation Tau tracers are now under investigation and are being processed in clinical trials.³⁵ With the aid of suitable screening, structure activity relationship (SAR) analysis, and structural optimization, [¹⁸F]MK-6240 was identified as the most potent Tau tracer, exhibiting high specificity and selectivity to NFTs.³⁶ [¹⁸F]MK-6240 is currently under phase I clinical trials.³⁷ More recently, other scaffolds, including 1,5-naphthyridine derivative [¹⁸F]JNJ-311,³⁸ isoquinoline derivative [¹⁸F]JNJ-067,^{39,40} imidazo[1,2-*a*]pyridine derivative [¹¹C]RO963, imidazo[1,2-*a*]pyrimidine derivative [¹¹C]RO643, pyrrolo[2,3-*b*:4,5-*c'*]dipyridine derivative [¹⁸F]RO948,^{41,42} naphthylethyldene malononitrile derivative [¹⁸F]1f,⁴³ and [¹⁸F]PI-2620^{44,45} and [¹⁸F]GTP1⁴⁶ as the derivatives of [¹⁸F]T807 and [¹⁸F]T808, were all evaluated as novel PET imaging probes for Tau.

We recently reported that the 2-phenylquinoxaline scaffold can recognize the β -sheet structure, including those of A β plaques and tangles. We developed A β imaging agents based on the scaffold.^{47–49} During those investigations, we found that some of these quinoxaline derivatives were capable of binding with NFTs on brain sections of AD patients in vitro. This greatly inspired us to develop Tau PET probes based on the optimization of the 2-phenylquinoxaline scaffold. We followed the successful optimization strategy of THK derivatives, in order to achieve an appropriate Tau targeting probe with high

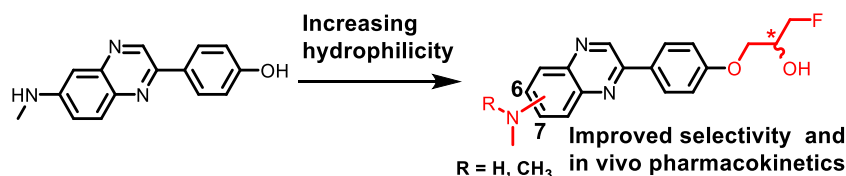


Figure 2. Design strategy for the 2-phenylquinoxaline scaffolds as PET probes of Tau.

binding affinity and selectivity over $A\beta$ plaques with low off-target binding and suitable in vivo pharmacokinetics. When a unique fluoropropanol side chain was introduced to the THK scaffold, to give [^{18}F]THK-5117²⁷ and [^{18}F]THK-5351,^{30,31} they showed higher selectivity for Tau and more favorable in vivo kinetics. In addition, during the development of [^{11}C]PBB3, the investigators showed that lower lipophilicity in their ligands synthesized improved the binding selectivity of Tau versus $A\beta$.⁵² In this study, we introduced the chiral fluoropropanol side chain at the phenolate position and *N,N*-dimethylamino/*N*-monomethylamino group at position 6 or 7 of the 2-phenylquinoxaline scaffold, to find compounds with increased binding affinity and selectivity toward NFTs (Figure 2). Thus, three pairs of ^{18}F -labeled chiral 2-phenylquinoxaline derivatives were designed, synthesized, and evaluated, as PET imaging probes for tangles.

EXPERIMENTAL SECTION

General Information. All reagents used for chemical synthesis and biological evaluation were purchased from commercial available suppliers; there is no further purification unless otherwise stated. Chemical reaction processes were monitored by Merck thin layer chromatography plates (aluminum sheets covered with silica gel 60 F₂₅₄ plates), and products were purified using flash column chromatography with silica gel (45–75 μm) matrix. ^1H NMR and ^{13}C NMR spectra were conducted on a Bruker Avance 400 MHz, JEOL JNM-ECZ 400 or 600 MHz spectrometer in CDCl_3 or deuterated dimethyl sulfoxide ($\text{DMSO-}d_6$) solutions at r.t., and the deuterated solvent resonance was employed as an internal standard. Chemical shifts (δ) are reported in ppm, coupling constants (J) are reported in hertz (Hz), and the multiplicity is defined by s (singlet), d (doublet), t (triplet) or m (multiplet). Low-resolution mass spectrometry (MS) spectra were acquired using a Thermo Surveyor MSQ Plus (ESI) instrument, and high-resolution mass spectra (HRMS) were acquired using a Thermo Scientific Q-Exactive (ESI) mass spectrometer. The fluorescence spectra were obtained using RF-5301PC spectrofluorophotometer (Shimadzu). The absolute fluorescence quantum yields were determined by Absolute PL Quantum Yield Spectrometer C11347 (Hamamatsu). The radioactivity was determined using an automatic γ -counter (WALLAC/Wizard 2480). The radioligands were purified using an SCL-20 AVP high-performance liquid chromatography (HPLC) system (Shimadzu) equipped with an SPD-20A UV detector ($\lambda = 254$ nm) and γ -radiation scintillation detector (Bioscan Flow Count 3200 NaI/PMT). The HPLC conditions were: a reverse-phase semipreparative Venusil MP C18 column (Bonna-Agela, 5 μm , 10 mm \times 250 mm), isocratic solvent system (phase B was acetonitrile, while phase A was water) with the flow rate at 4.0 mL/min. The optical purity was determined on a Primaide HPLC System (Hitach) equipped with a Chiralpak AS-RH column (Daicel, 5 μm , 4.6 \times 150 mm) eluted with an isocratic solvent system (phase A was

isopropyl alcohol, while phase B was hexane) with the flow rate at 0.5 mL/min. The fluorescence imaging was performed using an EVOS FL fluorescence microscope imaging system (Life Technologies) equipped with 4',6-diamidino-2-phenylindole (DAPI), green fluorescent protein (GFP), red fluorescent protein (RFP), and Cy5.0 filter sets. Autoradiography images were scanned using a Cyclone Plus storage phosphor system (PerkinElmer). In vivo micro-PET/CT imaging was performed on micro-PET/CT (Super Nova, PINGSENG Healthcare). Male ICR mice (5 weeks, 18–22 g, male), SD rats (8–9 weeks, 300–350 g, male), and WT mice (C57BL6, 12 months old, male) used for biodistribution and in vitro fluorescent staining were purchased from Vital River Laboratories. Post-mortem brain tissues of Tg-tau mice (C57BL6, rTg4510, 7 months old, female) were kindly provided by Xuanwu Hospital, Capital Medical University. Brain tissue samples from an autopsy confirmed the AD patients (91 years old, male, temporal lobe; 85 years old, male, entorhinal cortex) were obtained from the Chinese Brain Bank Center. All protocols involving the use of animals were granted and supervised by the animal care committee of Beijing Normal University.

Synthesis. *4-(6-Nitroquinoxalin-2-yl)phenol (1).* 4-Nitro-*o*-phenylenediamine (3.1 g, 20.0 mmol) was diluted in dimethyl sulfoxide (DMSO) (8 mL) and placed at 0 $^\circ\text{C}$, and then 2-bromo-4'-hydroxyacetophenone (4.3 g, 20.0 mmol) diluted in DMSO (5 mL) was added dropwise into the solution. The reaction mixture was placed at r.t. with stirring for 10 min. After collection, the precipitate was washed with 100 mL of EtOH and 200 mL of deionized water. Compound **1** was gained as a yellow crystalline solid (3.1 g, 58%). ^1H NMR (400 MHz, $\text{DMSO-}d_6$) δ 10.27 (s, 1H), 9.68 (d, $J = 4.5$ Hz, 1H), 8.81 (dd, $J = 13.2, 2.5$ Hz, 1H), 8.50 (dd, $J = 9.2, 2.6$ Hz, 1H), 8.29 (d, $J = 8.8$ Hz, 2H), 8.23 (t, $J = 9.0$ Hz, 1H), 6.98 (d, $J = 8.7$ Hz, 1H). Electrospray ionization mass spectrometry (ESIMS): m/z calcd for $\text{C}_{14}\text{H}_{10}\text{N}_3\text{O}_3$ 268.1; found 267.7, $[\text{M} + \text{H}]^+$.

4-(6-Aminoquinoxalin-2-yl)phenol (2). $\text{N}_2\text{H}_4 \cdot \text{H}_2\text{O}$ (5.1 g, 48.0 mmol) was added slowly into the solution of compound **1** (4.3 g, 16.1 mmol) and 10% Pd/C (0.8 g, 16.1 mmol) in 150 mL MeOH. The mixture was refluxed at 90 $^\circ\text{C}$ with stirring for 2 h. After the removal of Pd/C by filtration, the filtrate was concentrated under vacuum to yield crude compound **2**, which was recrystallized in MeOH to acquire a yellow crystalline solid (3.4 g, 89%). ^1H NMR (400 MHz, $\text{DMSO-}d_6$) δ 9.86 (s, 1H), 9.21 (s, 1H), 8.10 (d, $J = 8.7$ Hz, 2H), 7.78 (d, $J = 9.0$ Hz, 1H), 7.28 (dd, $J = 9.0, 2.4$ Hz, 1H), 6.99 (d, $J = 2.4$ Hz, 1H), 6.98 (s, 1H), 6.95 (s, 1H), 6.03 (s, 2H). ESIMS: m/z calcd for $\text{C}_{14}\text{H}_{12}\text{N}_3\text{O}$ 238.1; found 237.7, $[\text{M} + \text{H}]^+$.

4-(6-(Methylamino)quinoxalin-2-yl)phenol (3). To a solution of intermediate **2** (1.2 g, 5.0 mmol) and paraformaldehyde (0.6 g, 20.0 mmol) in MeOH (100 mL) was added CH_3ONa (5 M in MeOH) (2.0 mL, 10.0 mmol). The mixture was refluxed at 90 $^\circ\text{C}$ with stirring for 2 h. After this mixture was allowed to cool to r.t., NaBH_4 (0.8 g, 20.0 mmol) was

added slowly, and then the reaction mixture was refluxed for an additional 3 h. Water (200 mL) was added after the solvent was removed under reduced vacuum and the mixture was neutralized by HCl (1 M). After filtration, the crude product was collected, suspended in 100 mL of deionized water, and treated with ultrasound for 15 min. Compound 3 was collected by filtration as a yellow solid (1.2 g, 95%). ^1H NMR (400 MHz, DMSO- d_6) δ 9.78 (s, 1H), 9.16 (s, 1H), 8.03 (d, J = 8.2 Hz, 2H), 7.71 (d, J = 9.1 Hz, 1H), 7.23 (d, J = 9.1 Hz, 1H), 6.89 (d, J = 8.3 Hz, 2H), 6.71 (s, 1H), 6.59 (d, J = 4.4 Hz, 1H), 2.81 (d, J = 4.4 Hz, 3H). ESIMS: m/z calcd for $\text{C}_{15}\text{H}_{14}\text{N}_3\text{O}$ 252.1; found 252.2, $[\text{M} + \text{H}]^+$.

(R)-N-Methyl-2-(4-(oxiran-2-ylmethoxy)phenyl)quinoxalin-6-amine [(R)-4]. A mixture of compound 3 (0.5 g, 2.0 mmol), (R)-glycidyl 3-nitrobenzenesulfonate (0.6 g, 2.5 mmol), and CsF (0.9 g, 6.0 mmol) in 25 mL of dimethylformamide (DMF) was heated to 65 °C with stirring for 2 h. After it cooled to r.t., the reaction mixture was diluted with 150 mL of deionized water. After filtration, the precipitate was washed by deionized water three times. The crude product was purified by flash column chromatography (petroleum ether/ethyl acetate = 2:1, v/v) to generate the final product as a yellow solid (365.1 mg, 59%). ^1H NMR (400 MHz, CDCl_3) δ 9.05 (s, 1H), 8.13–7.98 (m, 2H), 7.89 (d, J = 9.1 Hz, 1H), 7.17 (dd, J = 9.1, 2.4 Hz, 1H), 7.12–7.01 (m, 3H), 4.32 (dd, J = 11.0, 3.1 Hz, 1H), 4.04 (dd, J = 11.0, 5.7 Hz, 1H), 3.40 (ddd, J = 7.0, 5.7, 2.9 Hz, 1H), 3.02 (s, 3H), 2.98–2.85 (m, 1H), 2.80 (dd, J = 4.9, 2.6 Hz, 1H). ESIMS: m/z calcd for $\text{C}_{18}\text{H}_{18}\text{N}_3\text{O}_2$ 308.1; found 308.3, $[\text{M} + \text{H}]^+$.

(S)-N-Methyl-2-(4-(oxiran-2-ylmethoxy)phenyl)quinoxalin-6-amine [(S)-4]. The procedures were similar to those used for the preparation of compound (R)-4, and the final product was gained as a yellow solid (378.4 mg, 62%). ^1H NMR (400 MHz, CDCl_3) δ 9.07 (s, 1H), 8.14–7.99 (m, 2H), 7.88 (d, J = 9.1 Hz, 1H), 7.15 (dd, J = 9.1, 2.5 Hz, 1H), 7.07 (d, J = 8.9 Hz, 2H), 7.01 (d, J = 2.2 Hz, 1H), 4.31 (dd, J = 11.0, 3.1 Hz, 1H), 4.04 (dd, J = 11.0, 5.7 Hz, 1H), 3.40 (ddd, J = 7.0, 5.8, 2.9 Hz, 1H), 3.01 (s, 3H), 2.98–2.91 (m, 1H), 2.80 (dd, J = 4.9, 2.6 Hz, 1H). ESIMS: m/z calcd for $\text{C}_{18}\text{H}_{18}\text{N}_3\text{O}_2$ 308.1; found 308.3, $[\text{M} + \text{H}]^+$.

(S)-1-Fluoro-3-(4-(6-(methylamino)quinoxalin-2-yl)phenoxy)propan-2-ol [(S)-5]. A solution of compound (R)-4 (283.4 mg, 0.9 mmol) and tetrabutylammonium fluoride (TBAF) (1 M in tetrahydrofuran (THF), 10.0 mL, 10.0 mmol) in anhydrous THF was placed at 90 °C with stirring and reflux for 6 h. After the completion of the reaction, the mixture was evaporated under vacuum and then purified by flash column chromatography (petroleum ether/ethyl acetate = 2:1, v/v). The final product was acquired as a yellow crystalline solid (230.6 mg, 76%). $[\alpha]_D^{22} +7.2$ (C 1.0, MeOH). ^1H NMR (400 MHz, CDCl_3) δ 9.08 (s, 1H), 8.08 (d, J = 8.0 Hz, 2H), 7.88 (d, J = 9.1 Hz, 1H), 7.15 (dd, J = 9.1, 2.6 Hz, 1H), 7.07 (d, J = 8.9 Hz, 2H), 7.01 (d, J = 2.1 Hz, 1H), 4.64 (dt, J = 47.0, 4.6 Hz, 2H), 4.38–4.26 (m, 1H), 4.21–4.12 (m, 2H), 3.01 (s, 3H). ^{13}C NMR (100 MHz, DMSO- d_6) δ 159.85, 151.06, 145.82, 144.18, 142.88, 136.21, 130.09, 129.79, 128.30, 123.12, 115.45, 101.54, 84.92 (d, J = 167.7 Hz), 68.78 (d, J = 7.7 Hz), 68.15 (d, J = 19.2 Hz), 30.06. HRESIMS: m/z calcd for $\text{C}_{18}\text{H}_{19}\text{FN}_3\text{O}_2$ 328.14558; found 328.14502, $[\text{M} + \text{H}]^+$.

(R)-1-Fluoro-3-(4-(6-(methylamino)quinoxalin-2-yl)phenoxy)propan-2-ol [(R)-5]. The procedures were similar to those used for the preparation of compound (S)-5; the final product was gained as a yellow crystalline solid (183.4 mg,

68%). $[\alpha]_D^{22} -7.2$ (C 1.0, MeOH). ^1H NMR (400 MHz, CDCl_3) δ 9.07 (s, 1H), 8.08 (d, J = 8.5 Hz, 2H), 7.89 (d, J = 8.9 Hz, 1H), 7.16 (d, J = 9.3 Hz, 1H), 7.10–6.97 (m, 3H), 4.63 (dt, J = 47.1, 5.2 Hz, 2H), 4.31 (d, J = 17.9 Hz, 1H), 4.17 (d, J = 4.9 Hz, 2H), 3.02 (s, 3H). ^{13}C NMR (100 MHz, DMSO- d_6) δ 159.85, 151.06, 145.82, 144.18, 142.88, 136.22, 130.10, 129.80, 128.30, 123.11, 115.44, 101.56, 84.93 (d, J = 166.7 Hz), 68.78 (d, J = 7.7 Hz), 68.16 (d, J = 19.1 Hz), 30.06. HRESIMS: m/z calcd for $\text{C}_{18}\text{H}_{19}\text{FN}_3\text{O}_2$ 328.14502; found 328.14558, $[\text{M} + \text{H}]^+$.

(R)-2-(4-((2,2-Dimethyl-1,3-dioxolan-4-yl)methoxy)phenyl)-N-methylquinoxalin-6-amine [(R)-6]. A mixture of compound 3 (756.4 mg, 3.0 mmol), (R)-(-)-2,2-dimethyl-4-(hydroxymethyl)-1,3-dioxolane-*p*-toluenesulfonate (1030.8 mg, 3.6 mmol), and CsF (1.4 g, 9.0 mmol) in 30 mL of DMF was placed at 65 °C for 2 h. After it cooled to r.t., the reaction mixture was diluted with 150 mL of deionized water, and the formed precipitate was washed by deionized water three times after filtration and collection. The crude product was purified by flash column chromatography (petroleum ether/ethyl acetate = 2:1, v/v) to give the final product as a yellow solid (1043.2 mg, 95%). ^1H NMR (400 MHz, CDCl_3) δ 9.08 (s, 1H), 8.06 (d, J = 7.6 Hz, 2H), 7.84 (d, J = 9.0 Hz, 1H), 7.12 (d, J = 9.2 Hz, 1H), 7.09–7.02 (m, 2H), 6.98 (s, 1H), 4.58–4.46 (m, 1H), 4.18 (dd, J = 15.2, 8.6 Hz, 1H), 4.14 (dd, J = 9.5, 5.5 Hz, 1H), 4.02 (dd, J = 9.4, 5.9 Hz, 1H), 3.94 (dd, J = 8.4, 5.9 Hz, 1H), 2.99 (s, 3H), 1.48 (s, 3H), 1.42 (s, 3H). ESIMS: m/z calcd for $\text{C}_{21}\text{H}_{24}\text{N}_3\text{O}_3$ 366.2; found 366.4, $[\text{M} + \text{H}]^+$.

(S)-2-(4-((2,2-Dimethyl-1,3-dioxolan-4-yl)methoxy)phenyl)-N-methylquinoxalin-6-amine [(S)-6]. The procedures were similar to those used for the preparation of compound (R)-6; the final product was gained as a yellow solid (1035.9 mg, 94%). ^1H NMR (400 MHz, CDCl_3) δ 9.06 (s, 1H), 8.19–7.95 (m, 2H), 7.82 (d, J = 9.0 Hz, 1H), 7.15 (d, J = 9.2 Hz, 1H), 7.04 (d, J = 8.7 Hz, 2H), 6.98 (s, 1H), 4.67–4.43 (m, 1H), 4.19 (dd, J = 8.5, 6.4 Hz, 1H), 4.11 (d, J = 5.4 Hz, 1H), 4.07–3.97 (m, 1H), 3.93 (dd, J = 8.5, 5.9 Hz, 1H), 2.98 (s, 3H), 1.48 (s, 3H), 1.42 (s, 3H). ESIMS: m/z calcd for $\text{C}_{21}\text{H}_{24}\text{N}_3\text{O}_3$ 366.2; found 366.3, $[\text{M} + \text{H}]^+$.

(R)-3-(4-(6-(Methylamino)quinoxalin-2-yl)phenoxy)propane-1,2-diol [(R)-7]. A solution of compound (R)-6 (1030.3 mg, 2.8 mmol) in 10 mL of THF and 30 mL of HCl (1 M) was placed at 90 °C with stirring and reflux for 30 min. After the completion of the reaction, the THF was evaporated under reduced vacuum, and the mixture was neutralized by 100 mL of saturated NaHCO_3 solution; the crystalline precipitate was filtrated to yield compound (R)-7 as a yellow solid (910.2 mg, 99%). ^1H NMR (400 MHz, DMSO- d_6) δ 9.21 (s, 1H), 8.13 (d, J = 8.6 Hz, 2H), 7.73 (d, J = 9.1 Hz, 1H), 7.24 (dd, J = 9.1, 1.7 Hz, 1H), 7.07 (d, J = 8.6 Hz, 2H), 6.72 (s, 1H), 6.62 (d, J = 4.8 Hz, 1H), 4.96 (d, J = 4.9 Hz, 1H), 4.67 (t, J = 5.4 Hz, 1H), 4.07 (dd, J = 9.8, 4.0 Hz, 1H), 3.93 (dd, J = 9.7, 6.2 Hz, 1H), 3.87–3.66 (m, 1H), 3.46 (t, J = 5.3 Hz, 2H), 2.81 (d, J = 4.8 Hz, 3H). ESIMS: m/z calcd for $\text{C}_{18}\text{H}_{20}\text{N}_3\text{O}_3$ 326.1; found 326.4, $[\text{M} + \text{H}]^+$.

(S)-3-(4-(6-(Methylamino)quinoxalin-2-yl)phenoxy)propane-1,2-diol [(S)-7]. The procedures were similar to those used for the preparation of compound (R)-7, and the final product was gained as a yellow solid (1064.3 mg, 99%). ^1H NMR (400 MHz, DMSO- d_6) δ 9.21 (s, 1H), 8.13 (d, J = 8.8 Hz, 2H), 7.73 (d, J = 9.1 Hz, 1H), 7.24 (dd, J = 9.1, 2.5 Hz, 1H), 7.07 (d, J = 8.9 Hz, 2H), 6.72 (d, J = 2.4 Hz, 1H), 6.62

(q, $J = 4.7$ Hz, 1H), 4.96 (d, $J = 5.2$ Hz, 1H), 4.66 (t, $J = 5.7$ Hz, 1H), 4.07 (dd, $J = 9.9$, 4.1 Hz, 1H), 3.93 (dd, $J = 9.9$, 6.2 Hz, 1H), 3.81 (td, $J = 12.2$, 5.6 Hz, 1H), 3.45 (t, $J = 5.7$ Hz, 2H), 2.81 (d, $J = 4.9$ Hz, 3H). ESIMS: m/z calcd for $C_{18}H_{20}N_3O_3$ 326.1; found 326.3, $[M + H]^+$.

(*S*)-2-(4-(2,3-Bis((*tert*-butyldimethylsilyloxy)propoxy)phenyl)-*N*-methylquinoxalin-6-amine [(*S*)-8]. To a solution of compound (*R*)-7 (0.6 g, 2.0 mmol) and *tert*-butyldimethylsilyl chloride (TBDMSCl) (1.8 g, 12.0 mmol) in acetonitrile (100 mL) was added imidazole (1.1 g, 16.0 mmol), and the mixture was placed at r.t. with stirring for 12 h. After evaporation to remove the solvent, the crude product was purified by flash column chromatography (petroleum ether/ethyl acetate = 3:1, v/v). The final product was gained as a yellow solid (1.0 g, 94%). 1H NMR (400 MHz, $CDCl_3$) δ 9.07 (s, 1H), 8.05 (d, $J = 8.6$ Hz, 2H), 7.88 (d, $J = 9.0$ Hz, 1H), 7.15 (d, $J = 9.1$ Hz, 1H), 7.09–6.89 (m, 3H), 4.18 (dd, $J = 9.5$, 3.3 Hz, 1H), 4.14–4.02 (m, 1H), 3.95 (dd, $J = 9.4$, 6.8 Hz, 1H), 3.67–3.65 (dd, $J = 5.6$, 2.9 Hz, 2H), 3.01 (s, 3H), 0.91 (d, $J = 1.5$ Hz, 18H), 0.12 (d, $J = 2.6$ Hz, 6H), 0.08 (s, 6H). ESIMS: m/z calcd for $C_{30}H_{48}N_3O_3Si_2$ 554.3; found 554.7, $[M + H]^+$.

(*R*)-2-(4-(2,3-Bis((*tert*-butyldimethylsilyloxy)propoxy)phenyl)-*N*-methylquinoxalin-6-amine [(*R*)-8]. The procedures were similar to those used for the preparation of compound (*S*)-8; the final product was gained as a yellow solid (1.0 g, 87%). 1H NMR (400 MHz, $CDCl_3$) δ 9.07 (s, 1H), 8.05 (d, $J = 8.9$ Hz, 2H), 7.89 (d, $J = 9.1$ Hz, 1H), 7.15 (dd, $J = 9.1$, 2.5 Hz, 1H), 7.05 (d, $J = 8.9$ Hz, 3H), 4.19 (dd, $J = 9.5$, 3.6 Hz, 1H), 4.09 (dt, $J = 10.2$, 6.6 Hz, 1H), 3.95 (dd, $J = 9.5$, 6.6 Hz, 1H), 3.67 (dd, $J = 5.9$, 3.2 Hz, 2H), 3.02 (s, 3H), 0.91 (d, $J = 2.3$ Hz, 18H), 0.12 (d, $J = 3.0$ Hz, 6H), 0.08 (d, $J = 0.7$ Hz, 6H). ESIMS: m/z calcd for $C_{30}H_{48}N_3O_3Si_2$ 554.3; found 554.6, $[M + H]^+$.

(*S*)-*tert*-Butyl (2-(4-(2,3-bis((*tert*-butyldimethylsilyloxy)propoxy)phenyl)quinoxalin-6-yl)(methyl)carbamate [(*S*)-9]. A solution of compound (*S*)-8 (1.0 g, 2.0 mmol) and (Boc)₂O (4.4 g, 20.0 mmol) in anhydrous THF was placed at 90 °C with stirring and reflux for 12 h. The solvent was evaporated under vacuum and purified by flash column chromatography (petroleum ether/ethyl acetate = 5:1, v/v). The final product was gained as a yellow solid (1.0 g, 81%). 1H NMR (400 MHz, $CDCl_3$) δ 9.25 (s, 1H), 8.16 (d, $J = 8.5$ Hz, 2H), 8.10 (d, $J = 9.1$ Hz, 1H), 7.99–7.64 (m, 2H), 7.09 (d, $J = 8.5$ Hz, 2H), 4.21 (dd, $J = 9.4$, 3.1 Hz, 1H), 4.10 (s, 1H), 3.97 (dd, $J = 8.9$, 7.2 Hz, 1H), 3.76–3.46 (m, 2H), 3.44 (s, 3H), 1.51 (s, 9H), 0.91 (d, $J = 1.5$ Hz, 18H), 0.12 (d, $J = 3.1$ Hz, 6H), 0.08 (s, 6H). ESIMS: m/z calcd for $C_{33}H_{56}N_3O_5Si_2$ 654.4; found 654.5, $[M + H]^+$.

(*R*)-*tert*-Butyl (2-(4-(2,3-bis((*tert*-butyldimethylsilyloxy)propoxy)phenyl)quinoxalin-6-yl)(methyl)carbamate [(*R*)-9]. The procedures were similar to those used for the preparation of compound (*S*)-9; the final product was gained as a yellow solid (1.2 g, 90%). 1H NMR (400 MHz, $CDCl_3$) δ 9.25 (s, 1H), 8.17–8.10 (m, 3H), 7.92–7.87 (m, 2H), 7.09 (d, $J = 8.7$ Hz, 2H), 4.21 (dd, $J = 9.6$, 3.4 Hz, 1H), 4.15–4.05 (m, 1H), 3.97 (dd, $J = 9.5$, 6.7 Hz, 1H), 3.67 (t, $J = 5.6$ Hz, 2H), 3.44 (s, 3H), 1.51 (s, 9H), 0.91 (d, $J = 2.5$ Hz, 18H), 0.12 (d, $J = 3.4$ Hz, 6H), 0.08 (d, $J = 0.7$ Hz, 6H). ESIMS: m/z calcd for $C_{33}H_{56}N_3O_5Si_2$ 654.4; found 654.6, $[M + H]^+$.

(*R*)-*tert*-Butyl (2-(4-(2,3-dihydroxypropoxy)phenyl)quinoxalin-6-yl)(methyl)carbamate [(*R*)-10]. A solution of compound (*S*)-9 (1.0 g, 1.5 mmol) and TBAF (1 M in THF,

4.5 mL, 4.5 mmol) in anhydrous THF was placed at 90 °C with stirring and reflux for 3 h. The solvent was evaporated under vacuum, and the product was purified by flash column chromatography (petroleum ether/ethyl acetate = 1:4, v/v). The final product was gained as a yellow solid (0.5 g, 74%). 1H NMR (400 MHz, $CDCl_3$) δ 9.25 (s, 1H), 8.17 (d, $J = 7.6$ Hz, 2H), 8.09 (dd, $J = 9.0$, 3.8 Hz, 1H), 7.91 (s, 2H), 7.10 (d, $J = 8.1$ Hz, 2H), 4.21–4.10 (m, 3H), 3.89 (dd, $J = 11.4$, 3.5 Hz, 1H), 3.80 (dd, $J = 11.4$, 5.0 Hz, 1H), 3.44 (s, 3H), 1.51 (s, 9H). ESIMS: m/z calcd for $C_{23}H_{28}N_3O_5$ 426.2; found 426.3, $[M + H]^+$.

(*S*)-*tert*-Butyl (2-(4-(2,3-dihydroxypropoxy)phenyl)quinoxalin-6-yl)(methyl)carbamate [(*S*)-10]. The procedures were similar to those used for the preparation of compound (*R*)-10; the final product was gained as a canary solid (0.6 g, 91%). 1H NMR (400 MHz, $CDCl_3$) δ 9.25 (s, 1H), 8.17 (d, $J = 8.9$ Hz, 2H), 8.11 (d, $J = 9.0$ Hz, 1H), 7.99–7.84 (m, 2H), 7.10 (d, $J = 8.9$ Hz, 2H), 4.16 (d, $J = 2.8$ Hz, 3H), 3.89 (dd, $J = 11.4$, 3.6 Hz, 1H), 3.80 (dd, $J = 11.4$, 5.0 Hz, 1H), 3.45 (s, 3H), 1.51 (s, 9H). ESIMS: m/z calcd for $C_{23}H_{28}N_3O_5$ 426.2; found 426.4, $[M + H]^+$.

(*S*)-3-(4-(6-((*tert*-Butoxycarbonyl)(methyl)amino)quinoxalin-2-yl)phenoxy)-2-hydroxypropyl 4-methylbenzenesulfonate [(*S*)-11]. Et_3N (2 mL) was added into the solution of compound (*R*)-10 (0.4 g, 1.0 mmol) and TsCl (0.2 g, 1.0 mmol) in anhydrous CH_2Cl_2 ; the mixture was placed at r.t. with stirring for 12 h. The solvent was evaporated under vacuum, and the product was purified by flash column chromatography (petroleum ether/ethyl acetate = 1:1, v/v). The product was gained as a yellow oil (160.1 mg, 28%). 1H NMR (400 MHz, $CDCl_3$) δ 9.25 (s, 1H), 8.16 (d, $J = 8.7$ Hz, 2H), 8.09 (d, $J = 9.0$ Hz, 1H), 7.88 (d, $J = 15.8$ Hz, 2H), 7.81 (d, $J = 8.3$ Hz, 2H), 7.34 (d, $J = 8.2$ Hz, 2H), 7.02 (d, $J = 8.7$ Hz, 2H), 4.40–4.18 (m, 3H), 4.10 (d, $J = 4.5$ Hz, 2H), 3.44 (s, 3H), 2.43 (s, 3H), 1.51 (s, 9H). ESIMS: m/z calcd for $C_{30}H_{34}N_3O_7S$ 580.2; found 580.4, $[M + H]^+$.

(*R*)-3-(4-(6-((*tert*-Butoxycarbonyl)(methyl)amino)quinoxalin-2-yl)phenoxy)-2-hydroxypropyl 4-methylbenzenesulfonate [(*R*)-11]. The procedures were similar to those used for the preparation of compound (*S*)-11; the final product was gained as a yellow oil (210.5 mg, 33%). 1H NMR (400 MHz, $CDCl_3$) δ 9.25 (s, 1H), 8.16 (d, $J = 7.6$ Hz, 2H), 8.10 (s, 1H), 7.91 (s, 2H), 7.82 (d, $J = 8.3$ Hz, 2H), 7.34 (d, $J = 8.4$ Hz, 2H), 7.02 (d, $J = 7.6$ Hz, 2H), 4.48–4.20 (m, 3H), 4.10 (d, $J = 4.4$ Hz, 2H), 3.45 (s, 3H), 2.43 (s, 3H), 1.51 (s, 9H). ESIMS: m/z calcd for $C_{30}H_{34}N_3O_7S$ 580.2; found 580.6, $[M + H]^+$.

(2*S*)-3-(4-(6-((*tert*-Butoxycarbonyl)(methyl)amino)quinoxalin-2-yl)phenoxy)-2-((tetrahydro-2*H*-pyran-2-yl)oxy)propyl 4-methylbenzenesulfonate [(*S*)-12]. A solution of compound (*S*)-11 (60.3 mg, 0.1 mmol), 3,4-dihydropyran (80.4 mg, 1.0 mmol), and pyridinium toluene-4-sulfonate (50.4 mg, 0.2 mmol) in anhydrous CH_2Cl_2 was placed at r.t. with stirring for 10 h. After the solvent was removed by evaporation under vacuum, the crude product was purified by flash column chromatography (petroleum ether/ethyl acetate = 2:1, v/v). The final product was gained as a yellow oil (60.6 mg, 90%). 1H NMR (400 MHz, $CDCl_3$) δ 9.25 (s, 1H), 8.16–8.10 (m, 3H), 7.90 (d, $J = 12.6$ Hz, 2H), 7.79 (dd, $J = 8.2$, 5.8 Hz, 2H), 7.30 (d, $J = 7.1$ Hz, 2H), 7.08–6.93 (m, 2H), 4.36–4.17 (m, 3H), 4.13–4.06 (m, 1H), 3.92–3.80 (m, 2H), 3.51–3.49 (m, 2H), 3.45 (d, $J = 1.3$ Hz, 3H), 2.41 (s, 3H), 1.82–1.67 (m, 2H), 1.53–1.51 (m, 4H), 1.51 (d, $J = 0.8$ Hz, 9H).

ESIMS: m/z calcd for $C_{35}H_{42}N_3O_8S$ 664.3; found 664.6, $[M + H]^+$.

(2*R*)-3-(4-(6-((*tert*-Butoxycarbonyl)(methylamino)quinoxalin-2-yl)phenoxy)-2-((tetrahydro-2*H*-pyran-2-yl)oxy)propyl 4-methylbenzenesulfonate [(*R*)-12]. The procedures were similar to those used for the preparation of compound (*S*)-12, and the final product was gained as a yellow oil (100.7 mg, 72%). 1H NMR (400 MHz, $CDCl_3$) δ 9.25 (s, 1H), 8.35–8.07 (m, 3H), 7.93 (d, $J = 11.6$ Hz, 2H), 7.80 (dd, $J = 11.5, 8.0$ Hz, 2H), 7.32 (dd, $J = 14.0, 8.1$ Hz, 2H), 7.08–6.86 (m, 2H), 4.38–3.99 (m, 5H), 3.90–3.70 (m, 2H), 3.49 (s, 1H), 3.45 (s, 3H), 2.41 (s, 3H), 1.78–1.70 (m, 4H), 1.52 (s, 2H), 1.52 (s, 9H). ESIMS: m/z calcd for $C_{35}H_{42}N_3O_8S$ 664.3; found 664.6, $[M + H]^+$.

N,N'-Dimethyl-4-nitrobenzene-1,3-diamine (13). A solution of 5-chloro-2-nitroaniline (12.5 g, 72.5 mmol) and K_2CO_3 (36.0 g, 26.1 mmol) in 150 mL of DMF was placed at 150 °C with vigorous stirring overnight. After the reaction, 500 mL of deionized water was added into the mixture, and the formed precipitate was gathered by filtration and washed by deionized water three times to receive the desired product as a yellow solid without further purification (12.4 g, 94%). 1H NMR (400 MHz, $CDCl_3$) δ 8.02 (d, $J = 9.7$ Hz, 1H), 6.15 (dd, $J = 9.7, 2.6$ Hz, 1H), 5.78 (d, $J = 2.6$ Hz, 1H), 3.05 (s, 6H). ESIMS: m/z calcd for $C_8H_{12}N_3O_2$ 182.1; found 182.2, $[M + H]^+$.

4-(6-(Dimethylamino)quinoxalin-2-yl)phenol (14) and 4-(7-(dimethylamino)quinoxalin-2-yl)phenol (21). In a solution of compound 13 (3.6 g, 20.0 mmol) in 150 mL of MeOH was added with 10% Pd/C (1.0 g, 20.0 mmol) at r.t.; the mixture was placed under H_2 atmosphere (1 atm). The mixture was placed at r.t. for 6 h with stirring. After the solvent was removed under vacuum, *N,N'*-dimethylbenzene-1,2,4-triamine was obtained as a pure white solid. Then a solution of 2-bromo-4'-hydroxyacetophenone (4.3 g, 20.0 mmol) diluted with 10 mL of DMSO was added. The reaction mixture was stirred at r.t. for 10 h. After the reaction, 150 mL of deionized water was added, and the product was extracted with ethyl acetate (10 \times 50 mL). The organic layer was combined and dried over anhydrous $MgSO_4$, then filtered and concentrated in vacuo. The crude product was purified by flash column chromatography (dichloromethane/ethyl acetate = 5:1, v/v) to give a mixture of regioisomers of 4-(6-(dimethylamino)quinoxalin-2-yl)phenol (14) and 4-(7-(dimethylamino)quinoxalin-2-yl)phenol (21). The regioisomers were separated by recrystallization with $H_2C_2O_4 \cdot 2H_2O$ in hot EtOH. After the mixture cooled to r.t., the oxalate of compound 14 precipitated first and was collected by filtration and washed by cold EtOH and neutralized with $NH_3 \cdot H_2O$ to give pure compound 14 as a yellow solid (0.6 g, 10%). 1H NMR (400 MHz, $DMSO-d_6$) δ 9.21 (s, 1H), 8.04 (d, $J = 8.4$ Hz, 2H), 7.81 (d, $J = 9.3$ Hz, 1H), 7.48 (dd, $J = 9.2, 1.9$ Hz, 1H), 6.95–6.86 (m, 3H), 3.06 (s, 6H). ESIMS: m/z calcd for $C_{16}H_{16}N_3O$ 266.1; found 266.3, $[M + H]^+$. The filtrate was neutralized by $NH_3 \cdot H_2O$ to gain pure compound 21 as a yellow solid (2.0 g, 30%). 1H NMR (400 MHz, $DMSO-d_6$) δ 9.05 (s, 1H), 8.12 (d, $J = 8.4$ Hz, 2H), 7.80 (d, $J = 9.3$ Hz, 1H), 7.41 (dd, $J = 9.2, 1.9$ Hz, 1H), 6.93 (dd, $J = 12.6, 5.1$ Hz, 3H), 3.08 (s, 6H). ESIMS: m/z calcd for $C_{16}H_{16}N_3O$ 266.1; found 266.2, $[M + H]^+$.

(*R*)-*N,N*-Dimethyl-2-(4-(oxiran-2-ylmethoxy)phenyl)quinoxalin-6-amine [(*R*)-15]. The procedures were similar to those used for the preparation of compound (*R*)-4; the final product was obtained as a yellow solid (547.3 mg, 85%). 1H

NMR (400 MHz, $CDCl_3$) δ 9.09 (s, 1H), 8.21–8.01 (m, 2H), 7.94 (d, $J = 9.3$ Hz, 1H), 7.39 (dd, $J = 9.4, 2.8$ Hz, 1H), 7.09 (d, $J = 2.8$ Hz, 1H), 7.06 (d, $J = 1.9$ Hz, 2H), 4.31 (dd, $J = 11.0, 3.1$ Hz, 1H), 4.04 (dd, $J = 11.0, 5.7$ Hz, 1H), 3.42–3.38 (m, 1H), 3.15 (s, 6H), 3.00–2.89 (m, 1H), 2.80 (dd, $J = 4.9, 2.6$ Hz, 1H). ESIMS: m/z calcd for $C_{19}H_{20}N_3O_2$ 322.1; found 322.3, $[M + H]^+$.

(*S*)-*N,N*-Dimethyl-2-(4-(oxiran-2-ylmethoxy)phenyl)quinoxalin-6-amine [(*S*)-15]. The procedures were similar to those used for the preparation of compound (*R*)-4; the final product was gained as a yellow solid (532.5 mg, 85%). 1H NMR (400 MHz, $CDCl_3$) δ 9.07 (s, 1H), 8.08 (d, $J = 8.9$ Hz, 2H), 7.96 (d, $J = 9.4$ Hz, 1H), 7.41 (dd, $J = 9.4, 2.7$ Hz, 1H), 7.13 (d, $J = 2.5$ Hz, 1H), 7.07 (d, $J = 8.8$ Hz, 2H), 4.32 (dd, $J = 11.0, 3.1$ Hz, 1H), 4.04 (dd, $J = 11.0, 5.7$ Hz, 1H), 3.40 (dt, $J = 8.6, 3.0$ Hz, 1H), 3.17 (s, 6H), 2.94 (t, $J = 4.5$ Hz, 1H), 2.80 (dd, $J = 4.9, 2.6$ Hz, 1H). ESIMS: m/z calcd for $C_{19}H_{20}N_3O_2$ 322.1; found 322.3, $[M + H]^+$.

(*S*)-1-(4-(6-(Dimethylamino)quinoxalin-2-yl)phenoxy)-3-fluoropropan-2-ol [(*S*)-16]. The procedures were similar to those used for the preparation of compound (*S*)-5; the final product was yielded as a yellow crystalline solid (187.2 mg, 85%). $[\alpha]_D^{22} +7.7$ (C 1.0, MeOH). 1H NMR (400 MHz, $CDCl_3$) δ 9.08 (s, 1H), 8.08 (d, $J = 8.8$ Hz, 2H), 7.95 (d, $J = 9.3$ Hz, 1H), 7.41 (dd, $J = 9.4, 2.7$ Hz, 1H), 7.12 (s, 1H), 7.07 (d, $J = 8.8$ Hz, 2H), 4.75–4.64 (m, 1H), 4.62–4.50 (m, 1H), 4.41–4.23 (m, 1H), 4.16 (d, $J = 4.8$ Hz, 2H), 3.16 (s, 6H). ^{13}C NMR (400 MHz, $DMSO-d_6$) δ 160.01, 151.00, 146.53, 143.44, 143.23, 135.56, 129.96, 129.84, 128.46, 120.50, 115.47, 105.36, 84.92 (d, $J = 167.7$ Hz), 68.80 (d, $J = 7.7$ Hz), 68.14 (d, $J = 19.1$ Hz), 40.57. HRESIMS: m/z calcd for $C_{19}H_{21}FN_3O_2$ 342.16123; found 342.16089, $[M + H]^+$.

(*R*)-1-(4-(6-(Dimethylamino)quinoxalin-2-yl)phenoxy)-3-fluoropropan-2-ol [(*R*)-16]. The procedures were similar to those used for the preparation of compound (*S*)-5; the product was gained as a yellow crystalline solid (168.2 mg, 82%). $[\alpha]_D^{22} -7.7$ (C 1.0, MeOH). 1H NMR (400 MHz, $CDCl_3$) δ 9.09 (s, 1H), 8.08 (dd, $J = 9.0, 2.4$ Hz, 2H), 7.94 (d, $J = 9.3$ Hz, 1H), 7.39 (dd, $J = 9.4, 2.6$ Hz, 1H), 7.07 (dt, $J = 9.1, 2.6$ Hz, 3H), 4.76–4.63 (m, 1H), 4.62–4.51 (m, 1H), 4.38–4.25 (m, 1H), 4.16 (dd, $J = 4.0, 1.7$ Hz, 2H), 3.15 (s, 6H). ^{13}C NMR (400 MHz, $DMSO-d_6$) δ 160.00, 150.98, 146.52, 143.42, 143.22, 135.56, 129.96, 129.83, 128.45, 120.47, 115.46, 105.36, 84.92 (d, $J = 167.7$ Hz), 68.79 (d, $J = 7.7$ Hz), 68.15 (d, $J = 19.1$ Hz), 40.56. HRESIMS: m/z calcd for $C_{19}H_{21}FN_3O_2$ 342.16123; found 342.16052, $[M + H]^+$.

(*R*)-2-(4-((2,2-Dimethyl-1,3-dioxolan-4-yl)methoxy)phenyl)-*N,N*-dimethylquinoxalin-6-amine [(*R*)-17]. The procedures were similar to those used for the preparation of compound (*R*)-6; the final product was gained as a yellow solid (673.1 mg, 94%). 1H NMR (400 MHz, $CDCl_3$) δ 9.09 (s, 1H), 8.12–8.04 (m, 2H), 7.94 (d, $J = 9.3$ Hz, 1H), 7.39 (d, $J = 9.3$ Hz, 1H), 7.10–7.05 (m, 3H), 4.52 (d, $J = 5.8$ Hz, 1H), 4.20 (dd, $J = 8.5, 6.4$ Hz, 1H), 4.14 (dd, $J = 9.5, 5.5$ Hz, 1H), 4.03 (dd, $J = 9.5, 5.8$ Hz, 1H), 3.94 (dd, $J = 8.5, 5.9$ Hz, 1H), 3.16 (d, $J = 3.0$ Hz, 6H), 1.49 (s, 3H), 1.42 (s, 3H). ESIMS: m/z calcd for $C_{22}H_{26}N_3O_3$ 380.2; found 380.4, $[M + H]^+$.

(*S*)-2-(4-((2,2-Dimethyl-1,3-dioxolan-4-yl)methoxy)phenyl)-*N,N*-dimethylquinoxalin-6-amine [(*S*)-17]. The procedures were similar to those used for the preparation of compound (*R*)-6; the final product was gained as a yellow solid (660.1 mg, 91%). 1H NMR (400 MHz, $CDCl_3$) δ 9.09 (s, 1H), 8.07 (d, $J = 8.9$ Hz, 2H), 7.95 (d, $J = 9.3$ Hz, 1H), 7.48–

7.30 (m, 1H), 7.11 (s, 1H), 7.07 (t, $J = 5.9$ Hz, 2H), 4.59–4.40 (m, 1H), 4.20 (dd, $J = 8.5, 6.4$ Hz, 1H), 4.14 (dd, $J = 9.5, 5.5$ Hz, 1H), 4.03 (dd, $J = 9.5, 5.8$ Hz, 1H), 3.94 (dd, $J = 8.5, 5.9$ Hz, 1H), 3.16 (s, 6H), 1.49 (s, 3H), 1.42 (s, 3H). ESIMS: m/z calcd for $C_{22}H_{26}N_3O_3$ 380.2; found 380.4, $[M + H]^+$.

(R)-3-(4-(6-(Dimethylamino)quinoxalin-2-yl)phenoxy)propane-1,2-diol [(*R*)-18]. The procedures were similar to those used for the preparation of compound (*R*)-7; the final product was gained as a yellow solid (594.2 mg, 96%). 1H NMR (400 MHz, DMSO- d_6) δ 9.27 (s, 1H), 8.17 (d, $J = 8.9$ Hz, 2H), 7.85 (d, $J = 9.3$ Hz, 1H), 7.50 (dd, $J = 9.4, 2.8$ Hz, 1H), 7.08 (d, $J = 8.9$ Hz, 2H), 6.97 (d, $J = 2.8$ Hz, 1H), 4.98 (d, $J = 4.8$ Hz, 1H), 4.68 (s, 1H), 4.07 (dd, $J = 9.9, 4.1$ Hz, 1H), 3.93 (dd, $J = 9.9, 6.2$ Hz, 1H), 3.81 (d, $J = 5.0$ Hz, 1H), 3.45 (t, $J = 4.8$ Hz, 2H), 3.09 (s, 6H). ESIMS: m/z calcd for $C_{19}H_{22}N_3O_3$ 340.2; found 340.3, $[M + H]^+$.

(S)-3-(4-(6-(Dimethylamino)quinoxalin-2-yl)phenoxy)propane-1,2-diol [(*S*)-18]. The procedures were similar to those used for the preparation of compound (*R*)-7; the final product was gained as a yellow solid (578.4 g, 94%). 1H NMR (400 MHz, DMSO- d_6) δ 9.27 (s, 1H), 8.17 (d, $J = 8.9$ Hz, 2H), 7.85 (d, $J = 9.3$ Hz, 1H), 7.50 (dd, $J = 9.4, 2.8$ Hz, 1H), 7.08 (d, $J = 8.9$ Hz, 2H), 6.97 (d, $J = 2.8$ Hz, 1H), 4.97 (s, 1H), 4.68 (s, 1H), 4.07 (dd, $J = 9.9, 4.1$ Hz, 1H), 3.93 (dd, $J = 9.9, 6.2$ Hz, 1H), 3.83–3.80 (m, 1H), 3.45 (d, $J = 5.7$ Hz, 2H), 3.09 (s, 6H). ESIMS: m/z calcd for $C_{19}H_{22}N_3O_3$ 340.2; found 340.4, $[M + H]^+$.

(S)-3-(4-(6-(Dimethylamino)quinoxalin-2-yl)phenoxy)-2-hydroxypropyl 4-methylbenzenesulfonate [(*S*)-19]. The procedures were similar to those used for the preparation of compound (*S*)-11; the desired product was gained as a yellow oil (265.2 mg, 38%). 1H NMR (400 MHz, $CDCl_3$) δ 9.08 (s, 1H), 8.06 (d, $J = 8.8$ Hz, 2H), 7.95 (d, $J = 9.3$ Hz, 1H), 7.80 (d, $J = 8.3$ Hz, 2H), 7.41 (d, $J = 9.4$ Hz, 1H), 7.32 (d, $J = 8.0$ Hz, 2H), 7.11 (s, 1H), 6.96 (d, $J = 8.6$ Hz, 2H), 4.39–4.12 (m, 3H), 4.07 (d, $J = 4.5$ Hz, 2H), 3.16 (s, 6H), 2.42 (s, 3H). ESIMS: m/z calcd for $C_{26}H_{28}N_3O_3S$ 494.2; found 494.4, $[M + H]^+$.

(R)-3-(4-(6-(Dimethylamino)quinoxalin-2-yl)phenoxy)-2-hydroxypropyl 4-methylbenzenesulfonate [(*R*)-19]. The procedures were similar to those used for the preparation of compound (*S*)-11; the desired product was gained as a yellow oil (193.6 mg, 36%). 1H NMR (400 MHz, $CDCl_3$) δ 9.08 (s, 1H), 8.06 (d, $J = 8.8$ Hz, 2H), 7.95 (d, $J = 9.4$ Hz, 1H), 7.81 (d, $J = 8.3$ Hz, 2H), 7.41 (dd, $J = 9.4, 2.7$ Hz, 1H), 7.33 (d, $J = 8.3$ Hz, 2H), 7.12 (s, 1H), 6.98 (t, $J = 7.0$ Hz, 2H), 4.28–4.22 (m, 3H), 4.07 (d, $J = 4.5$ Hz, 2H), 3.17 (s, 6H), 2.42 (s, 3H). ESIMS: m/z calcd for $C_{26}H_{28}N_3O_3S$ 494.2; found 494.4, $[M + H]^+$.

(2S)-3-(4-(6-(Dimethylamino)naphthalen-2-yl)phenoxy)-2-((tetrahydro-2H-pyran-2-yl)oxy)propyl 4-methylbenzenesulfonate [(*S*)-20]. The procedures were similar to those used for the preparation of compound (*S*)-12; the final product was gained as a yellow oil (127.4 mg, 87%). 1H NMR (400 MHz, $CDCl_3$) δ 9.06 (s, 1H), 8.05 (d, $J = 8.3$ Hz, 2H), 7.97 (d, $J = 9.3$ Hz, 1H), 7.79 (dd, $J = 8.2, 5.7$ Hz, 2H), 7.43 (dd, $J = 9.4, 2.6$ Hz, 1H), 7.29 (d, $J = 7.3$ Hz, 2H), 7.15 (s, 1H), 6.95 (dd, $J = 8.8, 5.7$ Hz, 2H), 4.42–4.13 (m, 4H), 4.12–3.99 (m, 2H), 3.52–3.46 (m, 2H), 3.18 (s, 6H), 2.40 (s, 3H), 1.82–1.59 (m, 2H), 1.53 (s, 4H). ESIMS: m/z calcd for $C_{31}H_{36}N_3O_6S$ 578.2; found 578.5, $[M + H]^+$.

(2R)-3-(4-(6-(Dimethylamino)naphthalen-2-yl)phenoxy)-2-((tetrahydro-2H-pyran-2-yl)oxy)propyl 4-methylbenzene-

sulfonate [(*R*)-20]. The procedures were similar to those used for the preparation of compound (*S*)-12, and the final product was gained as a yellow oil (100.7 mg, 90%). 1H NMR (400 MHz, $CDCl_3$) δ 9.05 (s, 1H), 8.04 (d, $J = 8.3$ Hz, 2H), 7.98 (d, $J = 9.1$ Hz, 1H), 7.84–7.74 (m, 2H), 7.45 (d, $J = 7.6$ Hz, 1H), 7.29 (d, $J = 7.9$ Hz, 2H), 7.18 (s, 1H), 6.95 (dd, $J = 8.8, 5.6$ Hz, 2H), 4.36–4.14 (m, 4H), 4.13–4.01 (m, 2H), 3.49 (s, 2H), 3.19 (s, 6H), 2.41 (s, 3H), 1.92–1.64 (m, 2H), 1.53 (s, 4H). ESIMS: m/z calcd for $C_{31}H_{36}N_3O_6S$ 578.2; found 578.4, $[M + H]^+$.

(R)-*N,N*-Dimethyl-3-(4-(oxiran-2-ylmethoxy)phenyl)quinoxalin-6-amine [(*R*)-22]. The procedures were similar to those used for the preparation of compound (*R*)-4; the final product was gained as a yellow solid (536.1 mg, 83%). 1H NMR (400 MHz, $CDCl_3$) δ 8.94 (s, 1H), 8.12 (d, $J = 8.8$ Hz, 2H), 7.90 (d, $J = 9.3$ Hz, 1H), 7.33 (dd, $J = 9.3, 2.8$ Hz, 1H), 7.15 (s, 1H), 7.08 (dd, $J = 6.9, 4.9$ Hz, 2H), 4.32 (dd, $J = 11.0, 3.1$ Hz, 1H), 4.04 (dd, $J = 11.0, 5.7$ Hz, 1H), 3.44–3.36 (m, 1H), 3.15 (s, 6H), 2.97–2.91 (m, 1H), 2.80 (dd, $J = 4.9, 2.6$ Hz, 1H). ESIMS: m/z calcd for $C_{19}H_{20}N_3O_2$ 322.1; found 322.2, $[M + H]^+$.

(S)-*N,N*-Dimethyl-3-(4-(oxiran-2-ylmethoxy)phenyl)quinoxalin-6-amine [(*S*)-22]. The procedures were similar to those used for the preparation of compound (*R*)-4; the final product was gained as a yellow solid (581.2 mg, 91%). 1H NMR (400 MHz, $CDCl_3$) δ 8.94 (s, 1H), 8.12 (d, $J = 8.8$ Hz, 2H), 7.89 (d, $J = 9.3$ Hz, 1H), 7.33 (dd, $J = 9.3, 2.8$ Hz, 1H), 7.13 (s, 1H), 7.10–7.03 (m, 2H), 4.32 (dd, $J = 11.0, 3.1$ Hz, 1H), 4.04 (dd, $J = 11.0, 5.7$ Hz, 1H), 3.44–3.36 (m, 1H), 3.15 (s, 6H), 2.95–2.88 (m, 1H), 2.80 (dd, $J = 4.9, 2.6$ Hz, 1H). ESIMS: m/z calcd for $C_{19}H_{20}N_3O_2$ 322.1; found 322.3, $[M + H]^+$.

(S)-1-(4-(7-(Dimethylamino)quinoxalin-2-yl)phenoxy)-3-fluoropropan-2-ol [(*S*)-23]. The procedures were similar to those used for the preparation of compound (*S*)-5; the final product was gained as a yellow crystalline solid (196.5 mg, 85%). $[\alpha]_D^{22} +7.5$ (C 1.0, MeOH). 1H NMR (400 MHz, $CDCl_3$) δ 8.94 (s, 1H), 8.14 (d, $J = 8.8$ Hz, 2H), 7.92 (d, $J = 9.3$ Hz, 1H), 7.35 (dd, $J = 9.3, 2.8$ Hz, 1H), 7.20 (s, 1H), 7.08 (d, $J = 8.9$ Hz, 2H), 4.63 (dt, $J = 47.0, 4.7$ Hz, 2H), 4.33–4.28 (m, 1H), 4.18–4.16 (dd, $J = 4.6, 2.6$ Hz, 2H), 3.17 (s, 6H). ^{13}C NMR (100 MHz, DMSO- d_6) δ 160.54, 151.65, 150.87, 143.97, 138.46, 135.17, 129.83, 129.58, 129.17, 119.39, 115.45, 105.33, 84.91 (d, $J = 167.7$ Hz), 68.82 (d, $J = 7.7$ Hz), 68.13 (d, $J = 19.1$ Hz), 40.54. HRESIMS: m/z calcd for $C_{19}H_{21}FN_3O_2$ 342.16123; found 342.16092, $[M + H]^+$.

(R)-1-(4-(7-(Dimethylamino)quinoxalin-2-yl)phenoxy)-3-fluoropropan-2-ol [(*R*)-23]. The procedures were similar to those used for the preparation of compound (*S*)-5; the final product was gained as a yellow crystalline solid (158.3 mg, 87%). $[\alpha]_D^{22} -7.5$ (C 1.0, MeOH). 1H NMR (400 MHz, $CDCl_3$) δ 8.94 (s, 1H), 8.18 (d, $J = 8.2$ Hz, 2H), 8.08 (d, $J = 8.8$ Hz, 1H), 7.94 (d, $J = 9.4$ Hz, 1H), 7.37 (dd, $J = 9.4, 2.4$ Hz, 1H), 7.10 (d, $J = 8.9$ Hz, 2H), 4.63 (dt, $J = 47.1, 5.0$ Hz, 2H), 4.34–4.29 (m, 1H), 4.18–4.17 (m, 2H), 3.19 (s, 6H). ^{13}C NMR (100 MHz, DMSO- d_6) δ 160.53, 151.64, 150.87, 143.96, 138.46, 135.17, 129.83, 129.57, 129.16, 119.37, 115.44, 105.33, 84.91 (d, $J = 167.7$ Hz), 68.82 (d, $J = 7.7$ Hz), 68.14 (d, $J = 19.1$ Hz), 40.53. HRESIMS: m/z calcd for $C_{19}H_{21}FN_3O_2$ 342.16123; found 342.16064, $[M + H]^+$.

(R)-3-(4-((2,2-Dimethyl-1,3-dioxolan-4-yl)methoxy)phenyl)-*N,N*-dimethylquinoxalin-6-amine [(*R*)-24]. The procedures were similar to those used for the preparation of

compound (R)-6; the final product was gained as a yellow solid (756.0 mg, 99%). ¹H NMR (400 MHz, CDCl₃) δ 8.93 (s, 1H), 8.13 (d, J = 3.2 Hz, 2H), 7.92 (s, 1H), 7.35 (s, 1H), 7.18 (s, 1H), 7.08 (s, 2H), 4.69–4.40 (m, 1H), 4.20 (dd, J = 8.5, 6.4 Hz, 1H), 4.14 (dd, J = 9.5, 5.5 Hz, 1H), 4.05 (d, J = 5.8 Hz, 1H), 3.94 (dd, J = 8.5, 5.9 Hz, 1H), 3.17 (s, 6H), 1.48 (s, 3H), 1.32 (s, 3H). ESIMS: *m/z* calcd for C₂₂H₂₆N₃O₃ 380.2; found 380.4, [M + H]⁺.

(S)-3-(4-((2,2-Dimethyl-1,3-dioxolan-4-yl)methoxy)phenyl)-N,N-dimethylquinoxalin-6-amine [(S)-24]. The procedures were similar to those used for the preparation of compound (R)-6; the final product was gained as a canary yellow solid (630.2 mg, 83%). ¹H NMR (400 MHz, CDCl₃) δ 8.93 (s, 1H), 8.13 (d, J = 8.7 Hz, 2H), 7.92 (d, J = 9.3 Hz, 1H), 7.35 (dd, J = 9.4, 2.4 Hz, 1H), 7.09 (d, J = 8.8 Hz, 2H), 4.51 (dd, J = 11.8, 5.9 Hz, 1H), 4.20 (dd, J = 8.5, 6.5 Hz, 1H), 4.14 (dd, J = 9.6, 5.5 Hz, 1H), 4.04 (dd, J = 9.5, 5.8 Hz, 1H), 3.93 (dd, J = 8.5, 5.9 Hz, 1H), 3.18 (s, 6H), 1.48 (s, 3H), 1.42 (s, 3H). ESIMS: *m/z* calcd for C₂₂H₂₆N₃O₃ 380.2; found 380.4, [M + H]⁺.

(R)-3-(4-(7-(Dimethylamino)quinoxalin-2-yl)phenoxy)propane-1,2-diol [(R)-25]. The procedures were similar to those used for the preparation of compound (R)-7; the final product was gained as a yellow solid (676.3 mg, 98%). ¹H NMR (400 MHz, DMSO-*d*₆) δ 9.10 (s, 1H), 8.22 (d, J = 8.5 Hz, 2H), 7.82 (d, J = 9.3 Hz, 1H), 7.43 (dd, J = 9.3, 2.0 Hz, 1H), 7.09 (d, J = 8.5 Hz, 2H), 6.96 (d, J = 1.9 Hz, 1H), 4.98 (d, J = 5.0 Hz, 1H), 4.69 (t, J = 5.6 Hz, 1H), 4.08 (dd, J = 9.8, 4.0 Hz, 1H), 3.94 (dd, J = 9.8, 6.2 Hz, 1H), 3.82 (dd, J = 10.1, 5.2 Hz, 1H), 3.46 (t, J = 5.6 Hz, 2H), 3.09 (s, 6H). ESIMS: *m/z* calcd for C₁₉H₂₂N₃O₃ 340.2; found 340.4, [M + H]⁺.

(S)-3-(4-(7-(Dimethylamino)quinoxalin-2-yl)phenoxy)propane-1,2-diol [(S)-25]. The procedures were similar to those used for the preparation of compound (R)-7; the final product was gained as a yellow solid (500.4 mg, 88%). ¹H NMR (400 MHz, DMSO-*d*₆) δ 9.28 (s, 1H), 8.19 (d, J = 8.5 Hz, 2H), 7.84 (d, J = 9.3 Hz, 1H), 7.47 (d, J = 9.2 Hz, 1H), 7.09 (t, J = 7.7 Hz, 2H), 6.97 (s, 1H), 4.98 (s, 1H), 4.68 (s, 1H), 4.09–4.05 (m, 1H), 4.02–3.88 (m, 1H), 3.81 (s, 1H), 3.46 (s, 2H), 3.09 (s, 6H). ESIMS: *m/z* calcd for C₁₉H₂₂N₃O₃ 340.2; found 340.5, [M + H]⁺.

(S)-3-(4-(7-(Dimethylamino)quinoxalin-2-yl)phenoxy)-2-hydroxypropyl 4-methylbenzenesulfonate [(S)-26]. The procedures were similar to those used for the preparation of compound (S)-11; the final product was gained as a yellow oil (260.5 mg, 38%). ¹H NMR (400 MHz, CDCl₃) δ 8.91 (s, 1H), 8.08–8.06 (m, 3H), 7.90 (d, J = 9.3 Hz, 1H), 7.79 (d, J = 8.3 Hz, 1H), 7.34–7.29 (m, 3H), 7.10 (d, J = 2.6 Hz, 1H), 7.07–7.02 (m, 1H), 6.94 (dd, J = 8.8, 3.9 Hz, 1H), 4.33–4.18 (m, 3H), 4.12 (d, J = 7.2 Hz, 1H), 4.05 (d, J = 4.5 Hz, 1H), 3.15 (s, 6H), 2.40 (s, 3H). ESIMS: *m/z* calcd for C₂₆H₂₈N₃O₅S 494.2; found 494.5, [M + H]⁺.

(R)-3-(4-(7-(Dimethylamino)quinoxalin-2-yl)phenoxy)-2-hydroxypropyl 4-methylbenzenesulfonate [(R)-26]. The procedures were similar to those used for the preparation of compound (S)-11; the final product was gained as a yellow oil (173.3 mg, 34%). ¹H NMR (400 MHz, CDCl₃) δ 8.92 (s, 1H), 8.21–7.99 (m, 2H), 7.90 (d, J = 9.3 Hz, 1H), 7.80 (d, J = 8.3 Hz, 2H), 7.35–7.30 (m, 3H), 7.11 (d, J = 2.5 Hz, 1H), 6.98–6.89 (m, 2H), 4.28–4.21 (m, 3H), 4.13–3.97 (m, 2H), 3.16 (s, 6H), 2.41 (s, 3H). ESIMS: *m/z* calcd for C₂₆H₂₈N₃O₅S 494.2; found 494.7, [M + H]⁺.

(2S)-3-(4-(7-(Dimethylamino)quinoxalin-2-yl)phenoxy)-2-((tetrahydro-2H-pyran-2-yl)oxy)propyl 4-methylbenzenesulfonate [(S)-27]. The procedures were similar to those used for the preparation of compound (S)-12; the final product was gained as a yellow oil (123.5 mg, 77%). ¹H NMR (400 MHz, CDCl₃) δ 8.94 (s, 1H), 8.11 (d, J = 8.7 Hz, 2H), 7.91 (d, J = 9.3 Hz, 1H), 7.79 (dd, J = 8.2, 5.6 Hz, 2H), 7.35 (dd, J = 9.3, 2.7 Hz, 1H), 7.32–7.27 (m, 2H), 7.22 (s, 1H), 7.08–7.06 (m, 1H), 6.96 (dd, J = 8.8, 5.8 Hz, 1H), 4.36–4.05 (m, 6H), 3.57–3.47 (m, 2H), 3.17 (s, 6H), 2.40 (s, 3H), 1.82–1.67 (m, 2H), 1.56–1.50 (m, 4H). ESIMS: *m/z* calcd for C₃₁H₃₆N₃O₆S 578.2; found 578.6, [M + H]⁺.

(2R)-3-(4-(7-(Dimethylamino)naphthalen-2-yl)phenoxy)-2-((tetrahydro-2H-pyran-2-yl)oxy)propyl 4-methylbenzenesulfonate [(R)-27]. The procedures were similar to those used for the preparation of compound (S)-12; the final product was gained as a yellow oil (64.7 mg, 74%). ¹H NMR (400 MHz, CDCl₃) δ 8.93 (s, 1H), 8.21 (s, 2H), 8.04 (d, J = 8.0 Hz, 1H), 7.97 (d, J = 10.3 Hz, 1H), 7.79 (dd, J = 8.2, 5.8 Hz, 2H), 7.40 (d, J = 7.6 Hz, 1H), 7.31 (d, J = 7.0 Hz, 2H), 7.06–6.88 (m, 2H), 4.40–4.14 (m, 4H), 4.12–4.06 (m, 2H), 3.50 (s, 2H), 3.23 (s, 6H), 2.42 (s, 3H), 1.53 (s, 4H), 1.26 (s, 2H). ESIMS: *m/z* calcd for C₃₁H₃₆N₃O₆S 578.2; found 578.6, [M + H]⁺.

Radiochemistry. [¹⁸F⁻] Fluoride trapped on a QMA cartridge was eluted with 1 mL (acetonitrile/H₂O, v/v = 4/1) of Kryptofix-222/K₂CO₃ solution (13 mg of Kryptofix-222 and 1.1 mg of K₂CO₃) into a 10 mL reaction vial. The vial was heated to 120 °C with nitrogen gas flow to remove solvent for 3 min, and then the residue was dried azeotropically with three separate additions of anhydrous acetonitrile (1 mL). After the drying, the appropriate solution of tosylated precursors (S)/(R)-12, (S)/(R)-20, or (S)/(R)-27 (3.0 mg) in anhydrous acetonitrile (600 μL) was transferred into the vial and heated to 100 °C for 7 min. Then 400 μL of aqueous HCl (1 M) was added and heated at 100 °C for an additional 5 min. After it cooled to r.t., the solution was neutralized by the addition of an aqueous solution of NaHCO₃ (1 M). The reaction mixture was diluted with 10 mL of deionized water and then passed through a preconditioned Sep-Pak Plus-C18 cartridge (Cleanert IC-C18, Bonna-Agela Technologies). The cartridge was washed with 10 mL of deionized water, and then the trapped product was eluted with acetonitrile (2 × 1 mL) and subjected to HPLC purification on a Venusil MP C18 reverse-phase column (5 μm, 10 × 250 mm; Green Technologies). The HPLC fraction containing the product was collected and concentrated under vacuum, and it was diluted with saline containing 10% ethanol for biological evaluation.

In Vitro Fluorescent Staining. Paraffin-embedded brain slices (8-μm) from Tg-tau (C57BL6, rTg4510, 7 months old, female, temporal lobe), WT mouse (C57BL6, 12 months old, male), and AD patients (91 years old, male, temporal lobe; 85 years old, male, entorhinal cortex) were used for multi-fluorescent staining studies. Brain slices were deparaffinized by fresh xylene for 5 min and washed with EtOH and water for 1 min. Then the brain slice was incubated with prepared solutions of fluorinated compounds (1 μM, 10% ethanol), DANIR 3b (1 μM, 10% ethanol), and DAPI (1 μg/mL, in phosphate-buffered saline (PBS)), respectively. The staining was performed at r.t. for 15 min and washed with 40% EtOH solution. Fluorescent images were acquired on an EVOS FL fluorescence microscope imaging system (Life Technologies) equipped with GFP, RFP and DAPI filter sets.

Immunofluorescent Staining. Immunofluorescent staining was performed on the brain slices from Tg-tau (C57BL6, rTg4510, 7 months old, female) and AD patients (91 years old, male, temporal lobe; 85 years old, male, entorhinal cortex). Deparaffinization was performed according to the same methods described above. All steps that involved staining were completed in the moist cassette at r.t. Antigen retrieval was implemented with immersion of the brain slices into 0.01 M citric acid/sodium citrate acid buffer (pH = 6.0) at 95 °C for 10 min. After they cooled to r.t., the brain slices were washed with PBS (0.1 μ M, pH = 7.4, 3 \times 5 min). The antigens were blocked by incubation of the brain slices with 3% bovine serum albumin for 2 h, and the blocking buffer was removed by PBS (0.1 μ M, pH = 7.4, 3 \times 5 min). Subsequently, the brain slices were treated with antiphospho-tau monoclonal antibody (AT8) (5 μ g/mL, Thermo scientific) at 4 °C for 20 h. After they were washed by PBS (0.1 μ M, pH = 7.4, 3 \times 5 min) at r.t., the brain slices were incubated with a secondary antibody (donkey antimouse IgG) (4 μ g/mL, Alexa Fluor594, Abcam plc) for 2 h. After the brain slices were washed by PBS (0.1 μ M, pH = 7.4, 3 \times 5 min), the staining results were acquired on an EVOS FL fluorescence microscope imaging system (Life Technologies) equipped with a Cy5.0 filter set.

In Vitro Autoradiography. The deparaffinized brain slices from an AD patient (85 years old, male, entorhinal cortex) were incubated with 7 MBq/mL of 18 F-labeled tracers (10% ethanol) alone or 18 F-labeled tracers with 200 nM blocking compound ((S)-16, THK-5317, or T807) at r.t. for 40 min and then washed briefly with a 25% EtOH aqueous solution. After they were dried, the slices were exposed to a medium phosphorus plate (PerkinElmer) for 30 min, and the in vitro autoradiography images were recorded by a Cyclone Plus storage phosphor system (PerkinElmer).

In Vitro Inhibition Binding Assay. [3 H]THK523, [3 H]T807, and [3 H]PIB were used as radioligands to quantitatively determine the binding affinity. The AD brain tissue was homogenized in an assay medium (0.1% Tween-20 in PBS) and diluted 500 times in volume. Aliquots (100 μ L) of this brain homogenates were transferred to 48 tubes. Then 100 μ L of solution of radioligand ([3 H]THK523, [3 H]T807, or [3 H]PIB, 10 Bq/ μ L) in an assay medium was added into the tube; 10 μ L of nonradiolabeled probes (10^{-5} to 10^{-10} M in DMSO) was added into each tube and diluted with an assay medium to the final volume of 1 mL. Then the mixture was vortexed and incubated at 37 °C for 2 h. After separation of the mixture with a cell harvester, the filter paper (Whatman, GF/B; preprocessed by 0.5% polyethylenimine solution) was washed with 3 mL of PBS three times and then placed in 7 mL plastic vials. Four milliliters of scintillation fluid was added to each plastic vial and vortexed until the filter was floating. After incubation overnight, the radioactivity of scintillation vials was counted. The data were analyzed by GraphPad Prism version 4.03 (GraphPad Software). The inhibition constant (K_i) was calculated using the Cheng-Prusoff equation⁵⁹

$$K_i = IC_{50}/(1 + [L]/K_d)$$

where [L] is the concentration (0.4 nM). K_d is the equilibrium dissociation constant of the control radioligand, and IC_{50} is the half-maximal inhibitory concentration. K_d was calculated by a "Scatchard analysis of homologous displacement" from multiple runs with self-displacement from an AD brain.

Distribution Coefficient (Log D) Determination. HPLC-purified tracer (120 MBq/mL, 100 μ L) was added

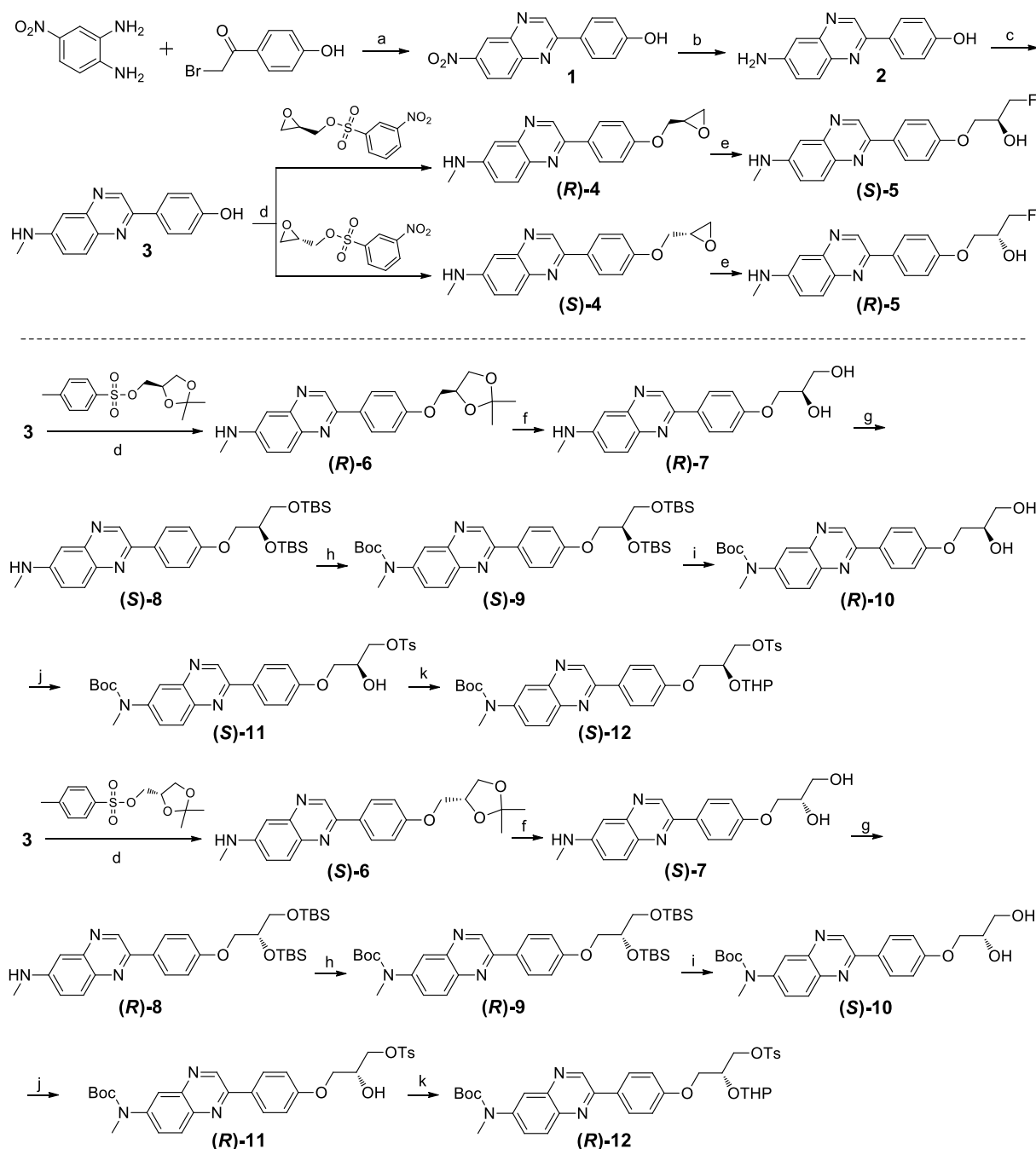
into a solution containing 3.0 mL of *n*-octanol and 3.0 mL of PBS (pH 7.4). The mixture was vortexed for 5 min and then centrifuged for 5 min at 3000 rpm/min. Samples from *n*-octanol (100 μ L) and PBS (500 μ L) were carefully taken in triplicate and tested by an automatic γ counter (WALLAC/Wizard 1470, PerkinElmer). Samples from the *n*-octanol layer (2.0 mL) were added into a solution containing 1.0 mL of *n*-octanol and 3.0 mL of PBS (pH 7.4) to repartition until consistent distribution coefficient values were obtained.

Ex Vivo Biodistribution Studies. The ex vivo biodistribution was performed on normal ICR mice (5 weeks, 18–22 g, male). 18 F-labeled ligand (6 MBq/mL, 100 μ L) in 10% EtOH saline solution was intravenously (*i.v.*) injected to each mouse through the tail vein. The mice ($n = 5$) were sacrificed by decapitation at 2, 10, 30, and 60 min after *i.v.* injection, respectively. The organs of interest were removed and weighed; the radioactive counts of the organs were recorded by an automatic γ counter (WALLAC/Wizard 1470, PerkinElmer). The percent dose per gram of wet tissue (% ID/g) was calculated by the ratio of the tissue counts to diluted aliquots of the injected dose. The mean \pm standard deviation (SD) was expressed as the uptake value for five parallel tests.

In Vivo Metabolism Studies. In vivo metabolism studies were performed on normal ICR mice rats (8–9 weeks, 300–350 g, male). The radiolabeled ligand (S)-[18 F]16 (18.5–74 MBq, 200 μ L) in 10% EtOH saline solution was injected via tail vein, and the mice were sacrificed at 10 and 60 min postinjection. The blood was collected as much as possible and centrifuged at 3000 rpm/min for 5 min to obtain plasma. Brain, liver, feces, and urine were also harvested and homogenized in 1–2 mL of acetonitrile. The obtained homogenates were passed through a disposable polypropylene (PP) syringe microporous filter (0.22 μ m) and added with 300 μ L of acetonitrile to further precipitate protein. The final samples were filtered and analyzed with a radio-HPLC (Shimadzu) equipped with an SPD-20A UV detector ($\lambda = 254$ nm) and γ -radiation scintillation detector (Bioscan Flow Count 3200 NaI/PMT). HPLC conditions: reverse-phase semipreparative Venusil MP C18 column (Bonna-Agela, 5 μ m, 10 mm \times 250 mm), 4 mL/min, acetonitrile/H₂O = 60%/40%.

In Vivo Micro-PET/CT Studies. In vivo micro-PET/CT imaging was performed in SD rats ($n = 2-3$, 300–350 g). The rat was anesthetized with 2.5% isoflurane gas in an oxygen flow during the imaging process and positioned on the bed of a micro-PET/CT scanner (Super Nova, PINGSENG Healthcare). An attenuation correlation was performed with an X-ray transmission scan, and then the radiolabeled ligands [18 F]THK-5351 or (S)-[18 F]16 (18.5 MBq, 2 mL) in 10% EtOH saline solution were *i.v.* bolus injected into the rat. Subsequently, dynamic brain PET scans (0 to 60 min) were started, and whole-body scans were also obtained at 60 min. We employed a three-dimensional ordered subset expectation maximization (3D OSEM) algorithm for image reconstruction. The time frames for brain PET imaging were 30 \times 120 s. Region of interest (ROI) outlines were drawn manually on the whole brain. The resulting ROI was then transferred to coregistered PET images. Standardized uptake values (SUVs) were calculated for all ROIs by a normalization of the injected dose and body weight. Time–Activity curves (TACs) were calculated from this.

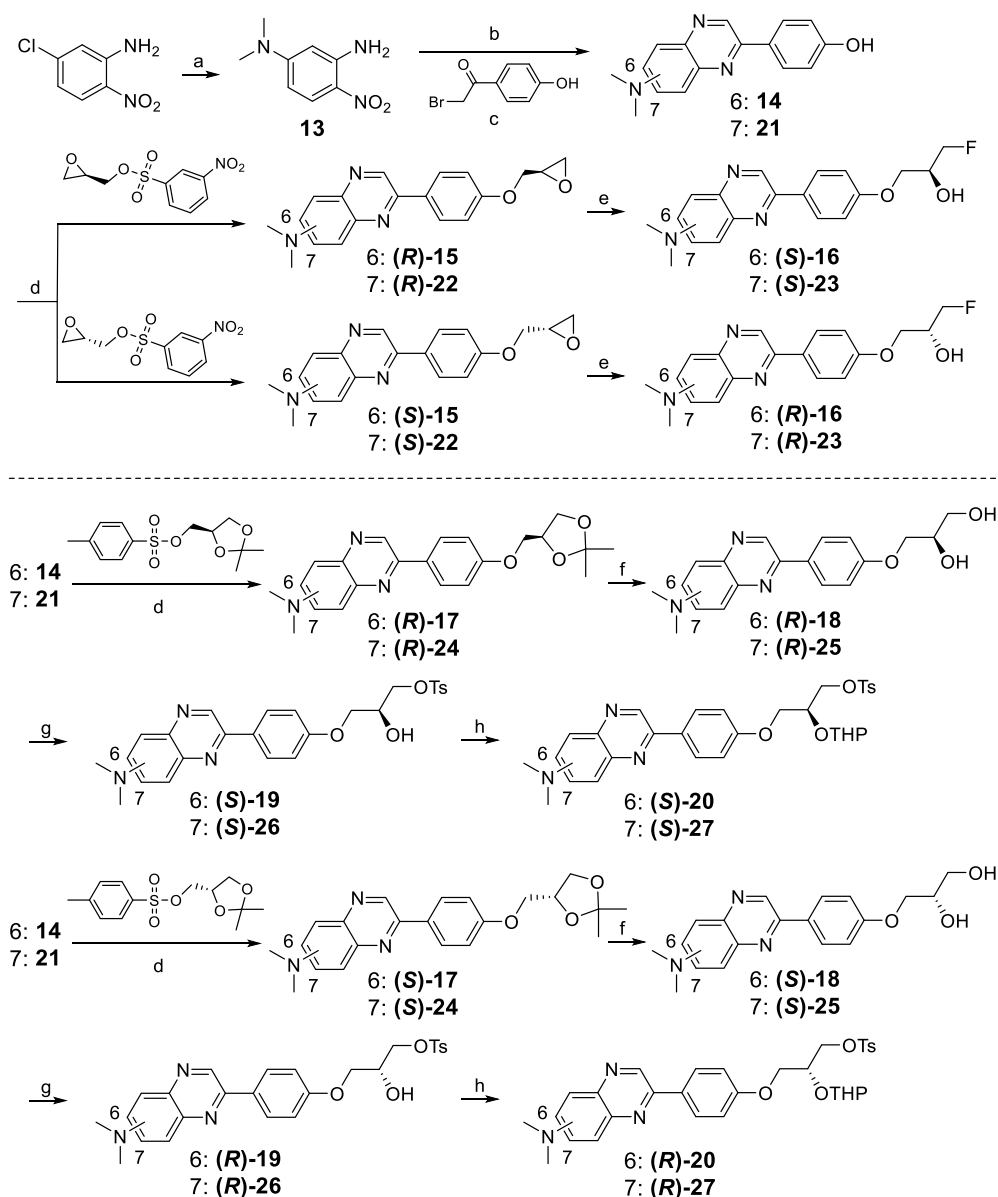
Mao-B Binding Assays in Liver Homogenates. The fresh liver tissue of an SD rat was washed in 0.2 M cold PBS

Scheme 1. Reagents and Conditions^a

^a(a) DMSO, r.t., 10 min, 58%; (b) $\text{N}_2\text{H}_4 \cdot \text{H}_2\text{O}$, Pd/C, MeOH, 90 °C, 2 h, 89%; (c) (1) $(\text{CH}_2\text{O})_m$, CH_3ONa , MeOH, 90 °C, 5 h, (2) NaBH_4 , 90 °C, 2 h, 95%; (d) CsF, DMF, 65 °C, 2h, (R)/(S)-4 = 59%/62%, (R)/(S)-6 = 95%/94%; (e) TBAF (1 M in THF), anhydrous THF, reflux for 6 h, (S)/(R)-5 = 76%/68%; (f) HCl (1 M), THF, 90 °C, reflux for 30 min, NaHCO_3 , (R)/(S)-7 = 99%/99%; (g) TBDMSCl, imidazole, acetonitrile, r.t., 12 h, (S)/(R)-8 = 94%/87%; (h) $(\text{Boc})_2\text{O}$, anhydrous THF, 90 °C, 12 h, (S)/(R)-9 = 81%/90%; (i) TBAF (1 M in THF), anhydrous THF, 90 °C, 3 h, (R)/(S)-10 = 74%/91%; (j) TsCl, TEA, CH_2Cl_2 , r.t., 12 h, (S)/(R)-11 = 28%/33%; (k) 3,4-dihydropyran, PPTS, CH_2Cl_2 , r.t., 10 h, (S)/(R)-12 = 90%/72%.

(−4 °C, pH = 7.6), followed by homogenization in 50 mL of sucrose (0.3 M, −4 °C) under an ice–water bath. Subsequently, the liver homogenates were centrifuged at 1000g for 10 min; the supernatants were separated and stored at −4 °C. The residues were further centrifuged at 1200g for 15 min with 10 mL of sucrose (0.3 M, −4 °C). All supernatants were gathered together and centrifuged at 10 000g for 15 min to obtain the deposition of mitochondrial

pellet after the removal of supernatants. The pellet was diluted with 4 mL of sucrose (0.3 M, −4 °C) and stored at −80 °C until required. The preparation of the enzyme–substrate solution was performed by dissolving 10 μL of 4-(trifluoromethyl)benzylamine in 9990 μL of PBS (0.2 M, pH 7.6). The chromogenic solution prepared for inclusion in the assay mixture contained vanillic acid (2 mM), 4-aminoantipyrene (1 mM), and peroxidase (250 IU/ml) in PBS (0.2

Scheme 2. Reagents and Conditions^a

^a(a) DMF, K₂CO₃, 150 °C, overnight, 94%; (b) H₂, Pd/C, MeOH, r.t., 6 h; (c) DMSO, r.t., 10 h, **14/21** = 10%/30%; (d) CsF, DMF, 65 °C, 2 h, (R)/(S)-**15** = 85%/85%, (R)/(S)-**17** = 94%/91%, (R)/(S)-**22** = 83%/91%, (R)/(S)-**24** = 99%/83%; (e) TBAF (1 M in THF), anhydrous THF, reflux for 6 h, (S)/(R)-**16** = 85%/82%, (S)/(R)-**23** = 85%/87%; (f) HCl (1M), THF, 90 °C, reflux for 30 min, (R)/(S)-**18** = 96%/94%, (R)/(S)-**25** = 98%/88%; (g) TsCl, TEA, CH₂Cl₂, r.t., 12 h, (S)/(R)-**19** = 38%/36%, (S)/(R)-**26** = 38%/34%; (h) 3,4-dihydropyran, PPTS, CH₂Cl₂, r.t., 10 h, (S)/(R)-**20** = 87%/90%, (S)/(R)-**27** = 77%/74%.

M, pH 7.6). Clorgyline solutions were prepared on a daily basis (1 μM). The assay was performed on a black 96-well plate (Costar), incubated at 37 °C for 30 min with 50 μL of tissue homogenates and 25 μL of clorgyline solution per well. After that, 50 μL of probe (concentration gradient manner) was added and incubated for another 30 min, with continuous incubation for 90 min with a successive addition of enzyme–substrate solution (120 μL) and chromogenic solutions (40 μL). The absorbance of each well was measured on InfiniteM200 pro microplate readers (Tecan) at 490 nm. The data were analyzed by GraphPad Prism version 4.03 (GraphPad Software).

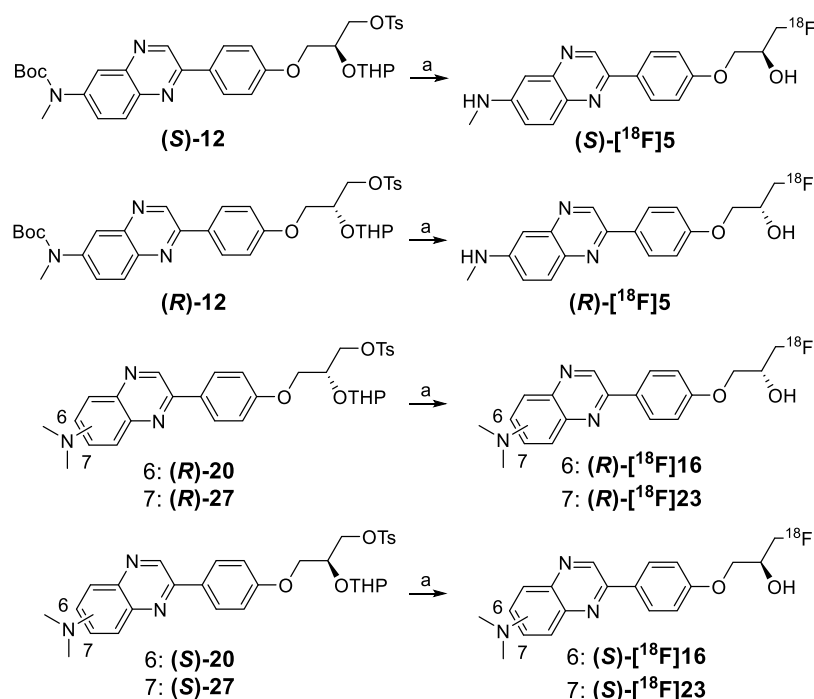
RESULTS AND DISCUSSION

Chemistry. The reference compounds for radioligands (S)-**5** and (R)-**5** were synthesized in five steps, with total overall yields of 22% and 21%, respectively. The 6-NO₂ substituted 2-phenylquinoxaline backbone (**1**) was synthesized as the major product by rapid cyclization of 4-nitro-*o*-phenylenediamine and 2-bromo-4'-hydroxyacetophenone in DMSO. Here, DMSO serves as both solvent for the reaction mixture and oxidant for the cyclized intermediate. After filtration, the compound was washed with EtOH (100 mL), which left a yellow crystal with high purity (Scheme 1). After an efficient catalytic reduction of the nitro group into an amino group to obtain **2**, the *N*-monomethylation was performed through a reductive methylation under basic conditions, to obtain

Table 1. Fluorescent Properties and Binding Affinity of the 2-Phenylquinoxaline-Based Tau Probes

probes	Φ , ^a %		$\lambda_{em}/\lambda_{ex}$ ^b (nm)		K_i ^c (nM) at			selectivity fold ^d	IC ₅₀ (μ M) for Mao-B	clog P ^e
	DCM	PBS	DCM	PBS	THK site	T807 site	PIB site			
(S)-5	58.6	12.3	493/411	554/418	36	>1000	87	2.4	1.21	2.98
(R)-5	58.0	16.2	493/410	553/419	4.1	630	125	30.5	0.33	2.98/2.36 ^f
(S)-16	70.7	4.6	500/426	578/441	10.3	611	356.3	34.6	>10	3.01/2.61 ^f
(R)-16	68.8	7.3	499/424	571/437	23	385	66	2.9	>10	3.01
(S)-23	22.4	4.2	502/422	584/425	13	>1000	94	7.2	>10	3.02
(R)-23	22.9	5.8	499/424	579/426	30	>1000	188	6.3	>10	3.02
THK-5351					2.9 ^g			0.7	0.49	3.02/2.71 ^f

^aAbsolute quantum yield measured in CH₂Cl₂ (100 nM) and PBS (100 nM). ^bEmission maxima determined in CH₂Cl₂ and PBS. ^c K_i values determined at the THK site, T807 site, and PIB site using AD brain homogenates. ^dSelectivity fold of K_i values for Tau over A β . ^eCalculated using the online ALOGPS 2.1 program. ^fMeasured log D value by testing the distribution coefficient between *n*-octanol and PBS. ^g K_d values adapted from ref 30.

Scheme 3. Reagents and Conditions^a

^a(a) (1) ¹⁸F⁻, K₂CO₃, Kryptofix-222, anhydrous acetonitrile, 100 °C; (2) (i) HCl (1 M), (ii) NaHCO₃.

compound 3. We selected (*R*)/(*S*)-glycidyl-3-nitrobenzenesulfonate with the highly efficient leaving group as the reagents to synthesize the chiral epoxides (*R*)/(*S*)-4 in moderate yields of 59–62%. The final fluorinated 2-phenylquinoxaline derivatives were obtained by a regioselective epoxy ring-opening reaction using tetra-*n*-butylammonium fluoride (TBAF) in yields of 68–76%, with an optical purity of the final products (*S*)/(*R*)-5 greater than 99% (Figure S1 and Table S1).

The precursors (*R*)/(*S*)-12 for radioligands (*S*)-5 and (*R*)-5 were synthesized in seven steps from compound 3, with total overall yields of 13% and 16%, respectively (Scheme 1). We used (*S*)-(+)-2,2-dimethyl-4-(hydroxymethyl)-1,3-dioxolane-*p*-toluenesulfonate and (*R*)-(–)-2,2-dimethyl-4-(hydroxymethyl)-1,3-dioxolane-*p*-toluenesulfonate, instead of (*S*)-(+)- or (*R*)-(–)-3-chloropropane-1,2-diol building block, to generate the chiral dioxolane derivatives (*R*)/(*S*)-6 in high yields of 94–95%, selectively, at the phenolate position instead of secondary aryl amino group. The isopropylidene group was removed by acidic hydrolysis to give the free propanediol derivatives (*R*)/

(*S*)-7 in high yields of 99%. To eliminate the influence of secondary aryl amino group on the radiofluorination reaction, we protected the amino group. First, the free dihydroxyl groups were protected by TBDMSCl, to give (*R*)/(*S*)-8. Second, the aryl methylamino group was protected using *tert*-butyloxycarbonyl (Boc) group, to give (*R*)/(*S*)-9. The silyl protecting group was removed selectively by TBAF to give (*R*)/(*S*)-10 in yields of 74–91%. The terminal less-hindered hydroxyl group in (*R*)/(*S*)-10 was selectively tosylated by *p*-tosyl chloride (TsCl) in CH₂Cl₂. To prevent the influence of the residual tertiary hydroxyl group in the radiofluorination, it was protected by a tetrahydropyranyl (THP) group, to give the desired precursors (*S*)/(*R*)-12.

The reference compounds for radioligand (*S*)/(*R*)-16 and (*S*)/(*R*)-23 were synthesized in four steps, with total overall yields of 7%, 7%, 20%, and 22%, respectively (Scheme 2). The *N,N*-dimethylamino group in (*S*)/(*R*)-16 and (*S*)/(*R*)-23 could not be synthesized from normal methylation reactions, including reductive amination and direct CH₃I methylation.

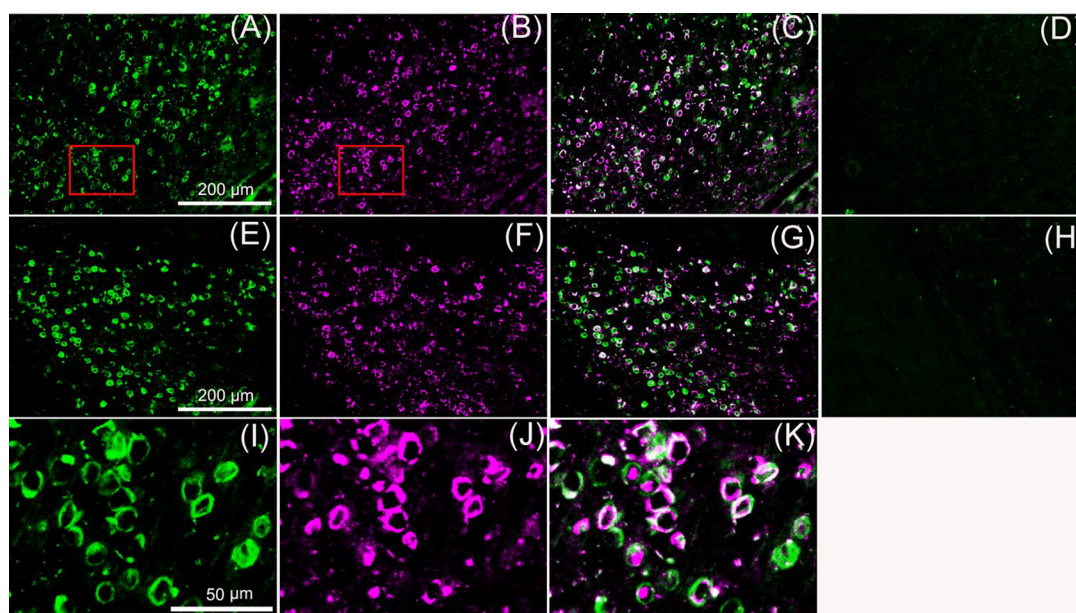


Figure 3. In vitro fluorescent staining on brain slices from Tg-tau mouse (C57BL6, rTg4510, 7 months old, female) by (R)-5 (A, GFP filter set, 20 \times) and (S)-16 (E, GFP filter set, 20 \times). The location of NFTs was confirmed by immunofluorescent staining using AT8 antibody (B, F, Cy5.0 filter set, 20 \times). Merged images of fluorescent staining and immunofluorescent staining results (C, G, and K). Fluorescent staining on brain slices from WT mouse (C57BL6, 12 months old, male) by (R)-5 (D, GFP filter set, 20 \times) and (S)-16 (H, GFP filter set, 20 \times). Red squares mark areas for magnification as presented in bottom panels (I, J).

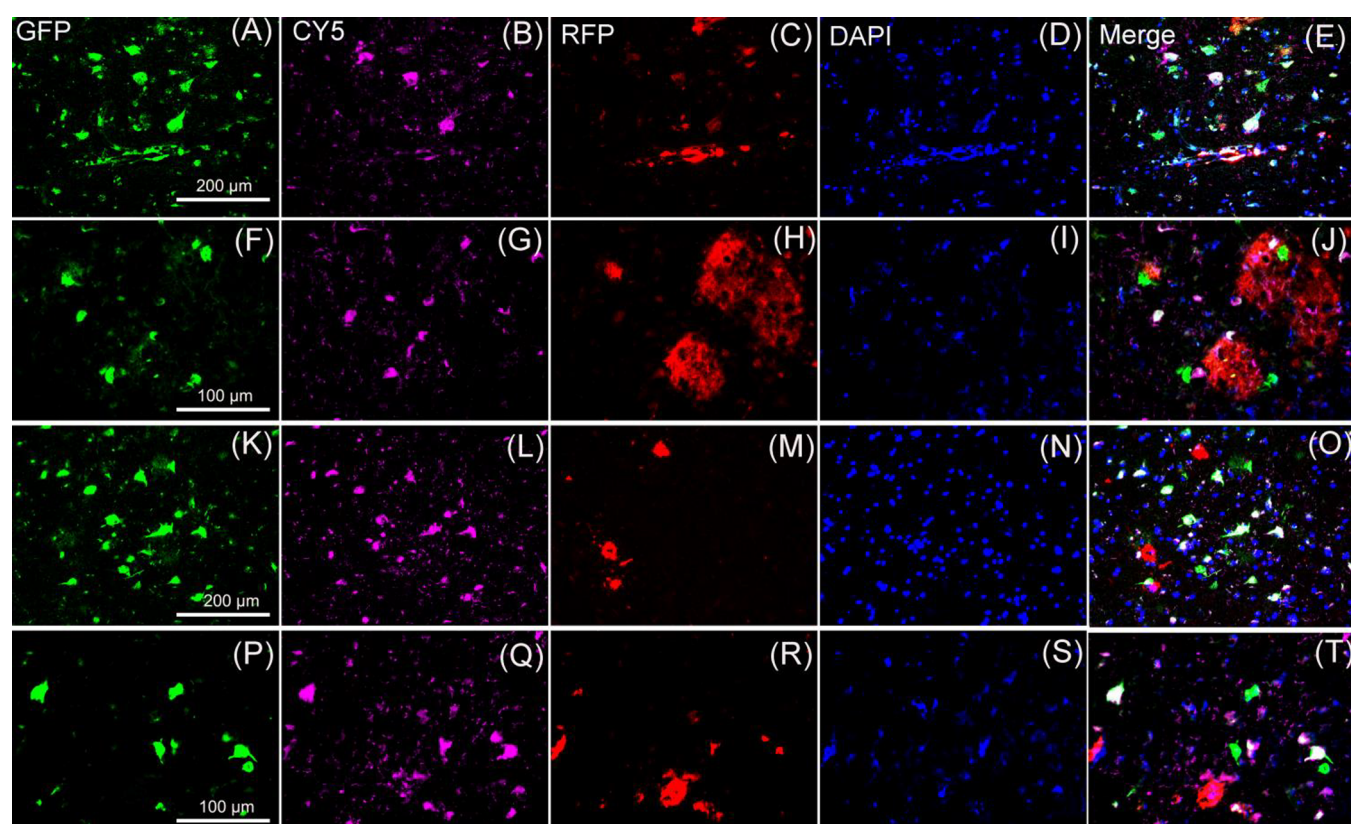


Figure 4. In vitro multifluorescent staining on brain slices from two AD patients. Staining results of (R)-5 (A, F) (1 μ M, 10% ethanol) and (S)-16 (K, P) (1 μ M, 10% ethanol) on GFP channel. The same brain slices were costained by AT8 antibody on Cy5.0 channel (B, G, L, Q); $A\beta$ probe DANIR 3b (1 μ M, 10% ethanol) on RFP channel (C, H, M, R); cell nucleus dye DAPI (1 μ g/mL, in PBS) on DAPI channel (D, I, N, S). Merged images for the corresponding staining results (E, J, O, T). Rows 1 and 3: (85 years old, male, entorhinal cortex; 20 \times); Rows 2 and 4: (91 years old, male, temporal lobe; 40 \times).

Thus, we designed a new synthetic route to introduce a dimethylamino group from the reaction of the commercially

available 5-chloro-2-nitroaniline in DMF, which serves as both solvent and dimethylamine precursor, to afford **13**. After a

catalytic reduction of the nitro group, the 2-phenylquinoxaline backbone was synthesized analogously as described in Scheme 1, to afford compounds **14** and **21**, depending on the position of the dimethylamino group (Scheme 2). Flash column chromatography was not effective to separate these two regioisomers, due to their similar structure and solubility in organic solvents. We separated these two regioisomers by a recrystallization of their oxalates in ethanol, due to their solubility difference. After it was neutralized with ammonium hydroxide, we obtained pure **14** and **21** with 10% and 30% yields, respectively. The remaining two steps for the synthesis of (S)/(R)-**16** and (S)/(R)-**23** are in accordance with those described in Scheme 1 (detailed in Scheme 2). Similarly, the precursors for radioligands (S)/(R)-**16** and (S)/(R)-**23**, namely, (S)/(R)-**20** and (S)/(R)-**27**, were synthesized in four steps from compounds **14** and **21**, with total overall yields of 30%, 28%, 28%, and 18%, respectively (Scheme 2). The optical purity of the final products (S)/(R)-**5**, (S)/(R)-**16**, and (S)/(R)-**23** was determined to be more than 99% by chiral HPLC analysis. All original ^1H NMR, ^{13}C NMR, MS, and HRMS spectra are described in the Supporting Information.

Fluorescent Properties. Compared with the 2-phenylquinoxaline derivatives,²⁶ 2-phenylquinoxaline derivatives displayed a stronger fluorescence with a red-shift (Table 1). The quantum yield of these compounds depends on both chemical structures and solvent used. The stronger electron-donating ability of the *N,N*-dimethylamino group gave both a higher quantum yield and a longer emission maxima than that of the *N*-monomethylamino group, (S/R)-**16** versus (S/R)-**5**. However, if the *N,N*-dimethylamino group is not in direct conjugation with the electron-poorer sp^2 hybridized nitrogen, the quantum yield is lower, (S/R)-**23** versus (S/R)-**16**. In addition, these ligands exhibited moderate solvatochromism, with a moderate red-shift of fluorescence emission maxima from CH_2Cl_2 to PBS. These ligands gave the highest quantum yield in CH_2Cl_2 , with $\sim 70\%$ quantum yield for (S/R)-**16**. However, the fluorescence was quenched significantly in PBS. These 2-phenylquinoxaline derivatives may serve as useful fluorescent probes for an in vitro detection of NFTs, due to their favorable fluorescent properties.

Radiochemistry. The ^{18}F -labeled tracers, (S/R)-[^{18}F]**5**, **16** and **23**, were prepared from the nucleophilic substitution of the tosylate in precursors, (S)/(R)-**12**, **20** and **27**, by [^{18}F]fluoride in the presence of K_2CO_3 and Kryptofix-222 (Scheme 3). After radiofluorination, removal of the *N*-*boc* or THP protecting groups by HCl (1 M) in the same reaction vessel was achieved in one pot yielding the crude tracers. The radiotracers were purified by semipreparative HPLC, and their identities were confirmed by HPLC coinjection analysis, with radiochemical yields greater than 20% and radiochemical purity greater than 98% (Figure S2 and Table S2). The molar activity of these tracers was calculated to be 90–123.5 GBq/ μmol .

In Vitro Histological Staining. In this study, multi-fluorescent staining of these 2-phenylquinoxaline derivatives was performed on brain slices from transgenic (Tg) mouse (C57BL6, rTg4510, 7 months old, female) and two autopsy-confirmed AD patients to demonstrate their selective binding with Tau deposits instead of $A\beta$ plaques. In vitro fluorescent staining is one of the rapid and efficient methods to screen fluorescent probes that have a high binding affinity and selectivity for specific targets at the tissue level. As mentioned before, these 2-phenylquinoxaline derivatives exhibited favor-

able fluorescent properties of high quantum yield and emission maxima around 550 nm in PBS, suitable for fluorescence staining. As shown in Figure 3, Figure 4, and Figures S3–S6, the hyperphosphorylated Tau deposits shown in the circled shape in the Tg-tau mouse and in the flame shape in the AD patients were illuminated clearly by (R)-**5** and (S)-**16** (GFP filter set). When the same tissue region was costained by DAPI to stain the cell nucleus (em: 461 nm, DAPI filter set) and DANIR **3b**⁵⁰ to specifically stain $A\beta$ (RFP filter set), no overlapped spots were observed in the merged images of the three staining images described above. This shows that our probes bind with protein targets other than $A\beta$. When the same tissue region was stained using immunofluorescence, with the first antibody, antiphospho-tau monoclonal antibody (AT8), and the secondary antibody, donkey antimouse IgG (Cy5.0 filter set), extensive overlap was observed in the merged images of the probes, (R)-**5** and (S)-**16**, and of the antibodies, confirming that our probes stain the hyperphosphorylated Tau deposits specifically. The AT8 antibody recognizes a phosphatase-sensitive epitope containing the phosphorylated Ser202 residue (numbering of human Tau40). Different from immunofluorescent staining, our probe recognizes the β -sheet structure of Tau tangles, which could explain that our probe performed more pronounced staining for Tau tangles than immunofluorescent staining. No specific signals were observed on brain slices from wild-type (WT) mouse. In addition, our probes stain NFTs consistently and rapidly, within 30 s even without washing. Compared with other time-consuming and expensive immunofluorescent staining, we believe that the fluorescent probes described here would also be useful for an in vitro detection of NFTs. Under the same experimental conditions, when we used PBB3³² as a probe for fluorescent staining, it displayed considerable staining of $A\beta$ plaques (Figure S7).

Determining Binding Constants. We determined the binding affinity of our probes using AD brain homogenates competing with three reference radioligands, namely, [^3H]THK-523, [^3H]T807, and [^3H]PIB. The first two radioligands are for the two different binding sites on Tau aggregates, respectively, and the last is for the binding site on $A\beta$ plaques. In some studies, the heparin-induced recombinant Tau fragments (K18 Δ 280 or K18) were usually used for in vitro affinity measurements.⁵¹ However, the inner conformation of a chemically induced Tau fibril may not be a reliable model for native NFTs, with differences including size, morphology, and hyperphosphorylation.⁵² The K_i values of our probes on different binding sites are shown in Table 1, and the probes exhibited a high affinity (<40 nM) on the THK site of NFTs, a moderate affinity (87–356.3 nM) on the PIB site of $A\beta$ plaques, and a poor affinity (>1000 nM) on the T807 site of NFTs. These results indicate that the 2-phenylquinoxaline scaffold shares the same THK binding site but not the T807 site of NFTs.⁵³ Since the concentration of Tau aggregates is ~ 5 –20 times lower than that of $A\beta$ aggregates, and since the two aggregates usually coexist in the brain of AD, a high affinity and selectivity for Tau aggregates are required for the PET imaging agents of Tau aggregates.^{54,55} Our probes, (R)-**5** and (S)-**16**, displayed a high affinity to NFTs ($K_i = 4.1$ and 10.3 nM) and outstanding selectivity over $A\beta$ aggregates (31- and 35-fold selectivity). They showed a similar affinity and selectivity with both THK-5351 (2.9 nM)³⁰ and T807 (2.6 nM).⁵³

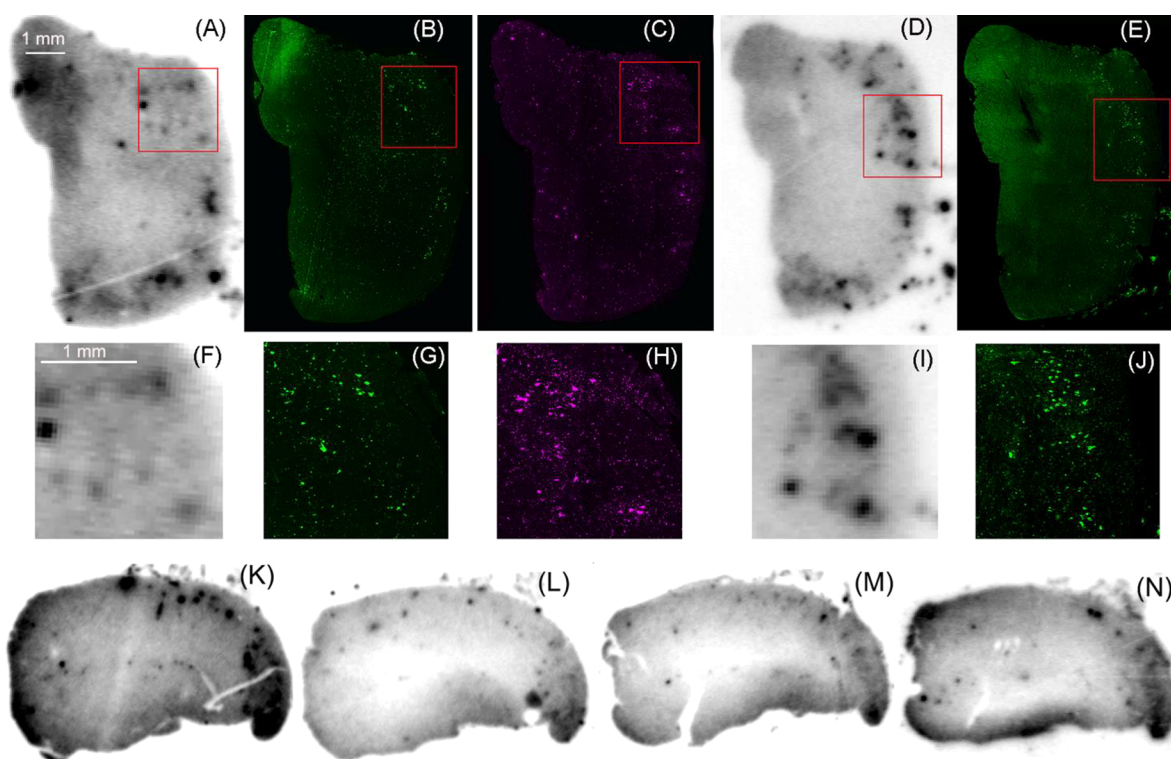


Figure 5. In vitro autoradiography of ^{18}F -radiolabeled ligands (R)- ^{18}F 5 (A) and (S)- ^{18}F 16 (D) on brain slices from an AD patient (85 years old, male; entorhinal cortex). The presence and location of NFTs were confirmed by fluorescent staining with the nonradiolabeled probes (R)-5 (B) and (S)-16 (E) or immunofluorescent staining using antiphospho-tau monoclonal antibody (AT8) (C). Red squares mark areas for magnification as presented in the middle panels (F, G, H, I, J). Totaling binding of (S)- ^{18}F 16 (K); self-blocking with 200 nM (S)-16 (L); blocking with 200 nM THK-5317 (M); blocking with 200 nM T807 (N).

Distribution Coefficient (Log D) Determination. To validate the effectiveness of introducing a fluoropropanol side chain to reduce lipophilicity, we determined the distribution coefficient between *n*-octanol and PBS (log *D*) and calculated the log *P* value using the online ALOGPS 2.1 program (clog *P*) for these 2-phenylquinoxaline derivatives. The lipophilicity values for (S)- ^{18}F 16 with a dimethylamino group (log *D* = 2.61 ± 0.05 , clog *P* = 3.01) and (R)- ^{18}F 5 with a monomethylamino group (log *D* = 2.36 ± 0.14 , clog *P* = 2.98) compared to dimethylamino derivatives ^{18}F 4a with a fluoropropylated chain⁴⁹ (log *D* = 3.14 ± 0.23 , clog *P* = 3.56) showed a significant decrease in lipophilicity by adding a fluoropropanol side chain, which may be the key factor that these probes possess high binding affinity and selectivity toward Tau over $A\beta$. In addition, these quinoxaline derivatives displayed similar lipophilicity values compared with those of ^{18}F THK-5351 (log *D* = 2.71 ± 0.05 , clog *P* = 3.02).

In Vitro Autoradiography. We used autoradiography studies of our radioligands on Tau-rich brain tissue from AD patient (entorhinal cortex), to confirm the specific binding ability of radiolabeled tracers with NFTs. As shown in Figure 5, a high density of specific radioactive signals in the entorhinal cortex was observed with high resolution to be NFTs, with their locations confirmed by fluorescent staining with the nonradiolabeled probes or immunofluorescent staining using antiphospho-tau monoclonal antibody (AT8). Moreover, (S)- ^{18}F 16 showed a strong signal with a high amount of displaceable binding in the region of high NFT load (Figure 5K) by self-blocking (Figure 5L) and THK-5317 blocking (Figure 5M) or partial blocking by T807 (Figure 5N).

Ex Vivo Biodistribution Studies. An ex vivo biodistribution study is a simple and efficient way to quantitatively determine the distribution of radiotracers in different organs, and it may also give information on metabolites. Three pairs of ^{18}F -labeled tracers [(S)/(R)- ^{18}F 5, 16, and 23] were investigated in normal ICR mice to evaluate their pharmacokinetic properties, as well as ^{18}F THK-5351 (leading compound of THK series). Similar to the requirements of PET $A\beta$ imaging agents, a desirable PET Tau imaging probe should possess a high initial uptake and fast washout in a normal brain. As shown in Figure 6A and Table 2, S3–S9, these radiotracers penetrated the blood-brain barrier (BBB) with greater than 6% ID/g in 2 min postinjection. The dimethylamino derivatives (S)/(R)- ^{18}F 16 showed the highest initial brain uptake (10.95% and 10.97% ID/g, respectively), which is pretty higher than ^{18}F THK-5351 ($6.46 \pm 0.43\%$ ID/g). Although the (R)/(S)-enantiomers showed a similar ability to cross the BBB, they differ in brain washout rate. The S-enantiomers (S)- ^{18}F 5, 16, and 23 with $\text{brain}_{2 \text{ min}}/\text{brain}_{60 \text{ min}} = 15.9, 6.5, \text{ and } 19.2$, respectively, showed a faster brain washout rate than the R-enantiomers (R)- ^{18}F 5, 16, and 23, with $\text{brain}_{2 \text{ min}}/\text{brain}_{60 \text{ min}} = 10.1, 3.8, \text{ and } 10.7$, respectively. The same pattern was also observed for the PET imaging of ^{18}F -labeled $A\beta$ imaging agents, as well as for the ^{18}F -labeled THK derivatives.^{6,30,56} As expected, the faster brain washout of the S-enantiomers also showed a faster excretion from intestine (Figure 6B). The brain washout rate also depends on lipophilicity and the rate of metabolism. The tracers, ((S)/(R)- ^{18}F 16), with dimethylamino group at the 6 position, showed a much slower brain washout than ((S)/(R)- ^{18}F 5), with a monomethylamino group. However, (R/S)-

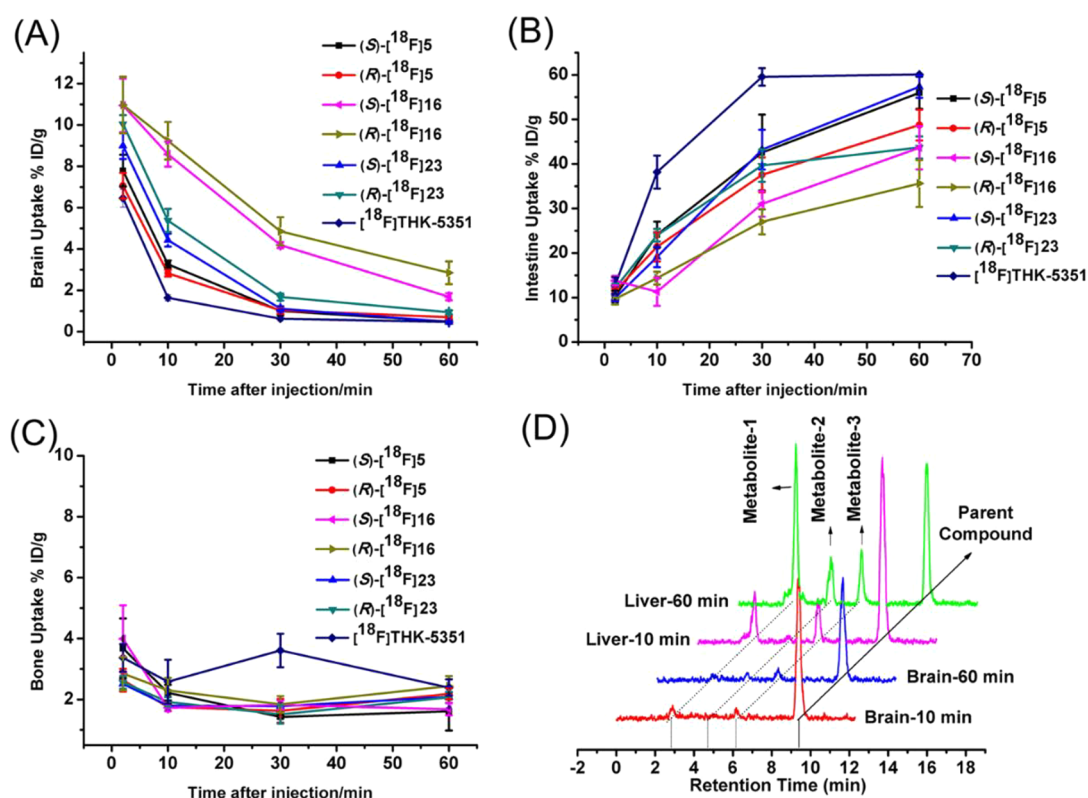


Figure 6. Ex vivo kinetic curves of brain (A), intestine (B), and bone (C) uptake for (S)/(R)-[¹⁸F]5, (S)/(R)-[¹⁸F]16, (S)/(R)-[¹⁸F]23, and [¹⁸F]THK-5351 in normal ICR mice at different time points postinjection. Error bars represent standard deviations for 5–6 mice at each time point. (D) HPLC profiles of the parent compound and metabolites extracted from the brain and liver of normal ICR mice after *i.v.* injection of (S)-[¹⁸F]16.

Table 2. Brain and Intestine Kinetics of ¹⁸F-Labeled Tracers in Normal ICR Mice

ligands	brain uptake ^a (% ID/g)		clearance rate	intestine uptake ^a (% ID)	
	2 min	60 min		2 min	60 min
(S)-[¹⁸ F]5	7.79 ± 0.77	0.49 ± 0.08	15.9	10.22 ± 1.32	55.99 ± 3.6
(R)-[¹⁸ F]5	7.06 ± 0.63	0.7 ± 0.08	10.1	11.43 ± 0.64	48.74 ± 3.45
(S)-[¹⁸ F]16	10.95 ± 1.29	1.69 ± 0.17	6.5	13.79 ± 1.09	43.65 ± 4.88
(R)-[¹⁸ F]16	10.97 ± 1.37	2.85 ± 0.55	3.8	9.67 ± 1.21	35.63 ± 5.28
(S)-[¹⁸ F]23	9.00 ± 0.64	0.47 ± 0.06	19.2	9.89 ± 0.67	57.35 ± 2.49
(R)-[¹⁸ F]23	10.05 ± 0.43	0.94 ± 0.10	10.7	12.03 ± 1.08	43.71 ± 2.48
[¹⁸ F]THK-5351	6.46 ± 0.43	0.47 ± 0.08	13.7	12.70 ± 1.85	60.12 ± 2.90

^aEach value was given as the mean ± SD for 5–6 mice at each time interval.

[¹⁸F]23 with a dimethylamino group at the 7 position showed a much faster brain washout rate than these with a dimethylamino group at the 6 position. The former may have a faster metabolic breakdown than the latter, because of the electronic conjugation difference discussed above. In addition, the brain clearance rate of [¹⁸F]THK-5351 ($\text{brain}_{2 \text{ min}}/\text{brain}_{60 \text{ min}} = 13.7$) is equivalent to that of the S-enantiomers of quinoxaline derivatives. Low levels of bone uptake (<4% ID/g) during the whole investigation indicate that our tracers and [¹⁸F]THK-5351 were stable against *in vivo* defluorination (Figure 6C).

In Vivo Metabolism and Micro-PET/CT Studies. To explore the *in vivo* biostability and metabolic mechanics, (S)-[¹⁸F]16 was *i.v.* injected into normal ICR mice, the mice were sacrificed at 10 and 60 min postinjection, and samples of the brain, liver, plasma, urine, and feces were collected and extracted with acetonitrile and analyzed with radio-HPLC. As

shown in Figure 6D and Table S10, three radioactive metabolites were observed, and they presented less lipophilicity than the parent compound with a shorter retention time in the HPLC profile. Liver is the main metabolic organ; the percent of metabolites increased from 10 to 60 min postinjection. It is worth mentioning that (S)-[¹⁸F]16 exhibited excellent biostability in the brain, and the percentage of the parent compound is more than 90% at 60 min postinjection. This also means that the polar metabolites generated in the liver cannot penetrate the BBB by bloodstream transportation. Furthermore, to make a direct comparison of brain kinetic properties between (S)-[¹⁸F]16 and [¹⁸F]THK-5351, dynamic micro-PET/CT studies were performed on SD rats. Although the peak brain uptake of (S)-[¹⁸F]16 (6 min) was slightly slower than that of [¹⁸F]THK-5351, (S)-[¹⁸F]16 exhibited a much higher BBB penetration than [¹⁸F]THK-5351 (SUV, 2.2 vs 1.3); the brain region

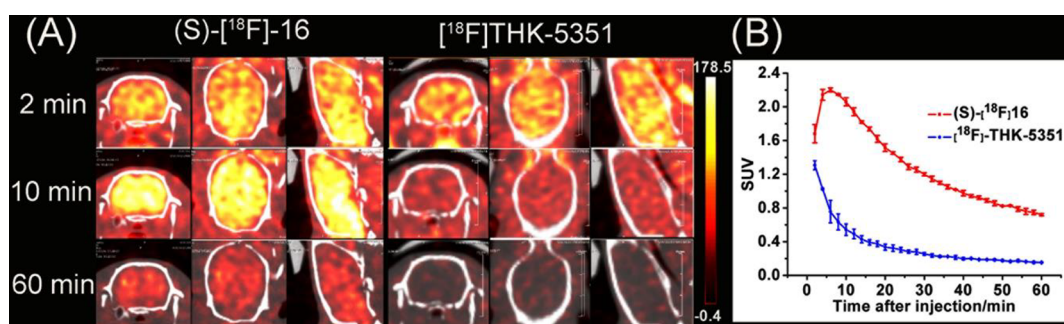


Figure 7. Dynamic micro-PET/CT study of (S)-[¹⁸F]16 and [¹⁸F]THK-5351 in SD rats ($n = 2-3$). (A) Summed PET images from rats overlaid on CT images in a transverse, coronal, and sagittal plane at time points of 2, 10, and 60 min. (B) Whole brain region time-activity curves after *i.v.* injection of tracers. Radioactivity concentration is expressed as SUV that is normalized to the injected dose and body weight.

became clearly visible after *i.v.* injection (Figure 7). However, a very high nonspecific retention in the submandibular gland of [¹⁸F]THK-5351 was observed from a scanning video at 2 and 10 min (see Supporting Information Video), which greatly suppressed the signals from the brain region. Although the washout rate of (S)-[¹⁸F]16 is slower than that of [¹⁸F]THK-5351 (3.1 vs 8.2), the radioactivity for (S)-[¹⁸F]16 in the brain still could be cleared at 60 min and concentrated in the intestine and stomach for these two tracers (see Figure 7 and Supporting Information Video). In addition, the results of *in vivo* PET studies are very consistent with *ex vivo* biodistribution and indicated (S)-[¹⁸F]16 possessed good pharmacokinetic properties.

In Vitro MAO-B Inhibition Binding Measurements. Monoamine oxidase B (MAO-B) is a flavoenzyme in the mitochondrial outer membrane and plays a major role in the metabolism of neuroactive and vasoactive amines. In the previous studies, the MAO-B binding was also considered as important off-target binding of THK probes.⁵⁷ Thus, the off-target effects of our Tau probes to MAO-B were assessed by an inhibition of the enzyme-substrate with the spectro-photometric assay, which was the similar method used for the test of MAO inhibition with JNJ-067.³⁹ As shown in Table 1 and Figure S8, (R/S)-5 and THK-5351 exhibited a moderate to poor inhibition ability (IC_{50} , 0.33–10 μ M) to MAO-B. To make a comparison, selegiline ($IC_{50} = 22.17 \pm 8.42$ nM), an irreversible MAO-B inhibitor, was also assayed under the same condition. Selegiline could efficiently inhibit the enzyme-substrate, and the results were consistent with the previously reported value ($IC_{50} = 19.60 \pm 0.86$ nM).⁵⁸ Compared with THK-5351 ($IC_{50} = 491.25$ nM), some of the quinoxaline derivatives displayed poor MAO-B affinity, for example, (R/S)-16 and (R/S)-23. Thus, the MAO-B off-target binding of these quinoxaline derivatives is expected to be very low.

In the present study, we designed, synthesized, and evaluated three pairs of ¹⁸F-labeled 2-phenylquinoxaline derivatives as novel Tau probes. Excellent fluorescent properties and *in vitro* fluorescent staining results validate that these probes could selectively bind to NFTs on brain sections from Tg-tau mouse and AD patients. Meanwhile, high quantum yield, selective binding, and fast labeling promoted them as fluorescence dyes to detect NFTs with high sensitivity *in vitro*. K_i values determined using competitive ligands ([³H]THK-523, [³H]T807, and [³H]PIB) on AD brain homogenates revealed that (R)-5 and (S)-16 possessed a high affinity to Tau tangles and selectivity over $A\beta$ plaques. Autoradiography studies on AD brain tissue demonstrated that NFTs could be

detected by (R)-[¹⁸F]5 and (S)-[¹⁸F]16, and the results were further confirmed by fluorescent and immunofluorescent staining. *Ex vivo* biodistribution in mice and micro-PET/CT studies in rats demonstrated that these probes could penetrate BBB sufficiently and actualize the brain region visible, and they showed fast washout from the normal brain quickly. Furthermore, (S)-[¹⁸F]16 displayed good stability in the brain and low inhibition to MAO-B. The parallel comparison between (S)-[¹⁸F]16 and [¹⁸F]THK-5351 revealed our tracers have many advantages such as high binding affinity, selectivity, initial brain uptake, and low off-target binding. On the basis of the results of these preclinical evaluations, (S)-16 satisfied the criteria to be promising PET probes for Tau imaging, and clinical validation studies of (S)-[¹⁸F]16 in AD patients and healthy subjects are undergoing; the results will be published in due course.

■ ASSOCIATED CONTENT

Supporting Information

The Supporting Information is available free of charge at <https://pubs.acs.org/doi/10.1021/acs.molpharmaceut.0c01078>.

- Additional figures, tables, NMR and MS spectra (PDF)
- Micro-PET/CT brain scanning video of [¹⁸F]THK-5351 at 2 min after *i.v.* injection (AVI)
- Micro-PET/CT brain scanning video of [¹⁸F]THK-5351 at 10 min after *i.v.* injection (AVI)
- Micro-PET/CT whole-body scanning video of (S)-[¹⁸F]16 at 60 min after *i.v.* injection (AVI)
- Micro-PET/CT whole-body scanning video of [¹⁸F]THK-5351 at 2 min after *i.v.* injection (AVI)

■ AUTHOR INFORMATION

Corresponding Authors

Mengchao Cui – Key Laboratory of Radiopharmaceuticals, Ministry of Education, Beijing Normal University, Beijing 100875, China; orcid.org/0000-0002-3488-7864; Email: cmc@bnu.edu.cn; Fax: +86-13811995064

Lisheng Cai – Molecular Imaging Branch, National Institute of Mental Health, National Institutes of Health, Bethesda 20892, Maryland, United States; Email: lishengcai@mail.nih.gov; Fax: +1-301-480-5112

Authors

Kaixiang Zhou – Key Laboratory of Radiopharmaceuticals, Ministry of Education, Beijing Normal University, Beijing 100875, China

Fan Yang – Key Laboratory of Radiopharmaceuticals, Ministry of Education, Beijing Normal University, Beijing 100875, China

Yuying Li – Key Laboratory of Radiopharmaceuticals, Ministry of Education, Beijing Normal University, Beijing 100875, China

Yimin Chen – Key Laboratory of Radiopharmaceuticals, Ministry of Education, Beijing Normal University, Beijing 100875, China

Xiaojun Zhang – Department of Nuclear Medicine, Chinese PLA General Hospital, Beijing 100853, China

Jinming Zhang – Department of Nuclear Medicine, Chinese PLA General Hospital, Beijing 100853, China

Junfeng Wang – Gordon Center for Medical Imaging, Department of Radiology, Massachusetts General Hospital/Harvard Medical School, Charlestown 02129, Massachusetts, United States

Jiapei Dai – Wuhan Institute for Neuroscience and Neuroengineering, South-Central University for Nationalities, Wuhan 430074, China; orcid.org/0000-0002-1474-5754

Complete contact information is available at:

<https://pubs.acs.org/10.1021/acs.molpharmaceut.0c01078>

Author Contributions

M.C. and K.Z. conceived and designed the experiments. K.Z., M.C., L.C., F.Y., Y.L., and Y.C. performed the experiments. K.Z., M.C., and L.C. analyzed the data. M.C., J.Z., X.Z., J.D., and L.C. contributed reagents, materials, and analysis tools. K.Z., M.C., J.W., and L.C. wrote the paper.

Funding

This work was funded by the Beijing Municipal Natural Science Foundation (No. 7182089) and the National Natural Science Foundation of China (No. U1967221).

Notes

The authors declare no competing financial interest.

ABBREVIATIONS USED

AD, Alzheimer's disease; $A\beta$, β -amyloid; NFTs, neurofibrillary tangles; PET, positron emission computed tomography; FDA, Food & Drug Administration; DMSO, dimethyl sulfoxide; r.t., room temperature; MeOH, methanol; DMF, *N,N*-dimethylformamide; TBAF, tetrabutylammonium fluoride; THF, tetrahydrofuran; HCl, hydrochloric acid; TBDMSCl, *tert*-butyldimethylsilyl chloride; Boc, *tert*-butyloxycarbonyl; TsCl, *p*-tosyl chloride; TEA, trimethylamine; PPTS, 4-toluenesulfonic acid pyridine salt; THP, tetrahydropyran; PBS, phosphate buffer saline; Tg, transgenic; WT, wild-type; SD, standard deviation; ID, injected dose; *i.v.*, intravenous; BBB, blood-brain barrier; NMR, nuclear magnetic resonance; J, coupling constant (in NMR spectrometry); MS, mass spectrometry; ESI, electron spray ionization; HRMS, high-resolution mass spectrometry; HPLC, high-performance liquid chromatography; DAPI, 4',6-diamidino-2-phenylindole; GFP, green fluorescent protein; ROI, region of interest; SUVs, standardized uptake values

REFERENCES

- (1) Khachaturian, Z. S. Diagnosis of Alzheimer's disease. *Arch. Neurol.* **1985**, *42*, 1097–1105.
- (2) Citron, M. Alzheimer's disease: strategies for disease modification. *Nat. Rev. Drug Discovery* **2010**, *9*, 387–398.

- (3) Brookmeyer, R.; Johnson, E.; Ziegler-Graham, K.; Arrighi, H. M. Forecasting the global burden of Alzheimer's disease. *Alzheimer's Dementia* **2007**, *3*, 186–191.

- (4) Trojanowski, J. Q.; Clark, C. M.; Schmidt, M. L.; Arnold, S. E.; Lee, V. M. Strategies for improving the postmortem neuropathological diagnosis of Alzheimer's disease. *Neurobiol. Aging* **1997**, *18*, S75–S79.

- (5) Jouanne, M.; Rault, S.; Voisin-Chiret, A. S. Tau protein aggregation in Alzheimer's disease: An attractive target for the development of novel therapeutic agents. *Eur. J. Med. Chem.* **2017**, *139*, 153–167.

- (6) Ariza, M.; Kolb, H. C.; Moechars, D.; Rombouts, F.; Andres, J. I. Tau Positron Emission Tomography (PET) Imaging: Past, Present, and Future. *J. Med. Chem.* **2015**, *58*, 4365–4382.

- (7) Shaw, L. M.; Vanderstichele, H.; Knapik-Czajka, M.; Clark, C. M.; Aisen, P. S.; Petersen, R. C.; Blennow, K.; Soares, H.; Simon, A.; Lewczuk, P.; Dean, R.; Siemers, E.; Potter, W.; Lee, V. M. Y.; Trojanowski, J. Q. Cerebrospinal Fluid Biomarker Signature in Alzheimer's Disease Neuroimaging Initiative Subjects. *Ann. Neurol.* **2009**, *65*, 403–413.

- (8) Aizenstein, H. J.; Nebes, R. D.; Saxton, J. A.; Price, J. C.; Mathis, C. A.; Tsopelas, N. D.; Ziolkowski, S. K.; James, J. A.; Snitz, B. E.; Houck, P. R.; Bi, W.; Cohen, A. D.; Lopresti, B. J.; DeKosky, S. T.; Halligan, E. M.; Klunk, W. E. Frequent amyloid deposition without significant cognitive impairment among the elderly. *Arch. Neurol.* **2008**, *65*, 1509–1517.

- (9) Jack, C. R.; Knopman, D. S.; Jagust, W. J.; Shaw, L. M.; Aisen, P. S.; Weiner, M. W.; Petersen, R. C.; Trojanowski, J. Q. Hypothetical model of dynamic biomarkers of the Alzheimer's pathological cascade. *Lancet Neurol.* **2010**, *9*, 119–128.

- (10) Villemagne, V. L.; Furumoto, S.; Fodero-Tavoletti, M.; Harada, R.; Mulligan, R. S.; Kudo, Y.; Masters, C. L.; Yanai, K.; Rowe, C. C.; Okamura, N. The challenges of tau imaging. *Future Neurol.* **2012**, *7*, 409–421.

- (11) Maccioni, R. B.; Farias, G.; Morales, I.; Navarrete, L. The revitalized tau hypothesis on Alzheimer's disease. *Arch. Med. Res.* **2010**, *41*, 226–231.

- (12) Arriagada, P. V.; Growdon, J. H.; Hedley-Whyte, E. T.; Hyman, B. T. Neurofibrillary tangles but not senile plaques parallel duration and severity of Alzheimer's disease. *Neurology* **1992**, *42*, 631–639.

- (13) Weingarten, M. D.; Lockwood, A. H.; Hwo, S. Y.; Kirschner, M. W. A protein factor essential for microtubule assembly. *Proc. Natl. Acad. Sci. U. S. A.* **1975**, *72*, 1858–1862.

- (14) Lee, G.; Neve, R. L.; Kosik, K. S. The microtubule binding domain of tau protein. *Neuron* **1989**, *2*, 1615–1624.

- (15) Lee, V. M.; Goedert, M.; Trojanowski, J. Q. Neurodegenerative tauopathies. *Annu. Rev. Neurosci.* **2001**, *24*, 1121–1159.

- (16) Isaac, M.; Vamvakas, S.; Abadie, E.; Jonsson, B.; Gispen, C.; Pani, L. Qualification opinion of novel methodologies in the predementia stage of Alzheimer's disease: cerebro-spinal fluid related biomarkers for drugs affecting amyloid burden. *Eur. Neuropsychopharmacol.* **2011**, *21*, 781–788.

- (17) Blennow, K.; Hampel, H.; Zetterberg, H. Biomarkers in amyloid-beta immunotherapy trials in Alzheimer's disease. *Neuropsychopharmacology* **2014**, *39*, 189–201.

- (18) Zetterberg, H.; Tullhög, K.; Hansson, O.; Minthon, L.; Londos, E.; Blennow, K. Low Incidence of Post-Lumbar Puncture Headache in 1,089 Consecutive Memory Clinic Patients. *Eur. Neurol.* **2010**, *63*, 326–330.

- (19) Xia, C.-F.; Arteaga, J.; Chen, G.; Gangadharmath, U.; Gomez, L. F.; Kasi, D.; Lam, C.; Liang, Q.; Liu, C.; Mocharla, V. P.; Mu, F.; Sinha, A.; Su, H.; Szardenings, A. K.; Walsh, J. C.; Wang, E.; Yu, C.; Zhang, W.; Zhao, T.; Kolb, H. C. [¹⁸F]T807, a novel tau positron emission tomography imaging agent for Alzheimer's disease. *Alzheimer's Dementia* **2013**, *9*, 666–676.

- (20) Zhang, W.; Arteaga, J.; Cashion, D. K.; Chen, G.; Gangadharmath, U.; Gomez, L. F.; Kasi, D.; Lam, C.; Liang, Q.; Liu, C.; Mocharla, V. P.; Mu, F.; Sinha, A.; Szardenings, A. K.; Wang, E.; Walsh, J. C.; Xia, C.; Yu, C.; Zhao, T.; Kolb, H. C. A highly

selective and specific PET tracer for imaging of tau pathologies. *J. Alzheimer's Dis.* **2012**, *31*, 601–612.

(21) Chien, D. T.; Bahri, S.; Szardenings, K.; Walsh, J.; Mu, F.; Su, M.-Y.; Shankle, W. R.; Elizarov, A.; Kolb, H. Early clinical PET imaging results with the novel PHF-Tau Radioligand [F-18]-T807. *J. Alzheimer's Dis.* **2013**, *34*, 457–468.

(22) Mintun, M.; Schwarz, A.; Joshi, A.; Shcherbinin, S.; Chien, D.; Elizarov, A.; Su, M.-Y.; Shankle, W.; Pontecorvo, M.; Tauscher, J.; Skovronsky, D.; Kolb, H. DT-01–02: Exploratory analyses of regional human brain distribution of the PET tau tracer F18-labeled T807 (AV-1541) in subjects with normal cognitive function or cognitive impairment thought to be due to Alzheimer's disease. *Alzheimer's Dementia* **2013**, *9*, P842–P842.

(23) Chien, D. T.; Szardenings, A. K.; Bahri, S.; Walsh, J. C.; Mu, F.; Xia, C.; Shankle, W. R.; Lerner, A. J.; Su, M. Y.; Elizarov, A.; Kolb, H. C. Early clinical PET imaging results with the novel PHF-tau radioligand [F18]-T808. *J. Alzheimer's Dis.* **2013**, *38*, 171–184.

(24) Kolb, H.; Attardo, G.; Mintun, M.; Chien, D.; Elizarov, A.; Conti, P.; Miller, C.; Joshi, A.; Skovronsky, D. DT-02–01: First case report: Image to autopsy correlation for tau imaging with [18F]-T808 (AV-680). *Alzheimer's Dementia* **2013**, *9*, P844–P845.

(25) Okamura, N.; Suemoto, T.; Furumoto, S.; Suzuki, M.; Shimadzu, H.; Akatsu, H.; Yamamoto, T.; Fujiwara, H.; Nemoto, M.; Maruyama, M.; Arai, H.; Yanai, K.; Sawada, T.; Kudo, Y. Quinoline and benzimidazole derivatives: candidate probes for in vivo imaging of tau pathology in Alzheimer's disease. *J. Neurosci.* **2005**, *25*, 10857–10862.

(26) Fodero-Tavoletti, M. T.; Okamura, N.; Furumoto, S.; Mulligan, R. S.; Connor, A. R.; McLean, C. A.; Cao, D.; Rigopoulos, A.; Cartwright, G. A.; O'Keefe, G.; Gong, S.; Adlard, P. A.; Barnham, K. J.; Rowe, C. C.; Masters, C. L.; Kudo, Y.; Cappai, R.; Yanai, K.; Villemagne, V. L. 18F-THK523: a novel in vivo tau imaging ligand for Alzheimer's disease. *Brain* **2011**, *134*, 1089–1100.

(27) Okamura, N.; Furumoto, S.; Harada, R.; Tago, T.; Yoshikawa, T.; Fodero-Tavoletti, M.; Mulligan, R. S.; Villemagne, V. L.; Akatsu, H.; Yamamoto, T.; Arai, H.; Iwata, R.; Yanai, K.; Kudo, Y. Novel 18F-labeled arylquinoline derivatives for noninvasive imaging of tau pathology in Alzheimer disease. *J. Nucl. Med.* **2013**, *54*, 1420–1427.

(28) Villemagne, V. L.; Furumoto, S.; Fodero-Tavoletti, M. T.; Mulligan, R. S.; Hodges, J.; Harada, R.; Yates, P.; Piguet, O.; Pejotka, S.; Dore, V.; Yanai, K.; Masters, C. L.; Kudo, Y.; Rowe, C. C.; Okamura, N. In vivo evaluation of a novel tau imaging tracer for Alzheimer's disease. *Eur. J. Nucl. Med. Mol. Imaging* **2014**, *41*, 816–826.

(29) Okamura, N.; Furumoto, S.; Fodero-Tavoletti, M. T.; Mulligan, R. S.; Harada, R.; Yates, P.; Pejotka, S.; Kudo, Y.; Masters, C. L.; Yanai, K.; Rowe, C. C.; Villemagne, V. L. Non-invasive assessment of Alzheimer's disease neurofibrillary pathology using 18F-THK5105 PET. *Brain* **2014**, *137*, 1762–1771.

(30) Harada, R.; Okamura, N.; Furumoto, S.; Furukawa, K.; Ishiki, A.; Tomita, N.; Tago, T.; Hiraoka, K.; Watanuki, S.; Shidahara, M.; Miyake, M.; Ishikawa, Y.; Matsuda, R.; Inami, A.; Yoshikawa, T.; Funaki, Y.; Iwata, R.; Tashiro, M.; Yanai, K.; Arai, H.; Kudo, Y. 18F-THK5351: A Novel PET Radiotracer for Imaging Neurofibrillary Pathology in Alzheimer Disease. *J. Nucl. Med.* **2016**, *57*, 208–214.

(31) Hsiao, I. T.; Lin, K. J.; Huang, K. L.; Huang, C. C.; Chen, H. S.; Wey, S. P.; Yen, T. C.; Okamura, N.; Hsu, J. L. Biodistribution and Radiation Dosimetry for the Tau Tracer (18F)-THK-5351 in Healthy Human Subjects. *J. Nucl. Med.* **2017**, *58*, 1498–1503.

(32) Maruyama, M.; Shimada, H.; Suhara, T.; Shinotoh, H.; Ji, B.; Maeda, J.; Zhang, M.-R.; Trojanowski, J. Q.; Lee, V. M. Y.; Ono, M.; Masamoto, K.; Takano, H.; Sahara, N.; Iwata, N.; Okamura, N.; Furumoto, S.; Kudo, Y.; Chang, Q.; Saido, T. C.; Takashima, A.; Lewis, J.; Jang, M.-K.; Aoki, I.; Ito, H.; Higuchi, M. Imaging of Tau Pathology in a Tauopathy Mouse Model and in Alzheimer Patients Compared to Normal Controls. *Neuron* **2013**, *79*, 1094–1108.

(33) Hashimoto, H.; Kawamura, K.; Igarashi, N.; Takei, M.; Fujishiro, T.; Aihara, Y.; Shiomi, S.; Muto, M.; Ito, T.; Furutsuka, K.; Yamasaki, T.; Yui, J.; Xie, L.; Ono, M.; Hatori, A.; Nemoto, K.;

Suhara, T.; Higuchi, M.; Zhang, M. R. Radiosynthesis, photoisomerization, biodistribution, and metabolite analysis of 11C-PBB3 as a clinically useful PET probe for imaging of tau pathology. *J. Nucl. Med.* **2014**, *55*, 1532–1538.

(34) Ni, R.; Ji, B.; Ono, M.; Sahara, N.; Zhang, M. R.; Aoki, I.; Nordberg, A.; Suhara, T.; Higuchi, M. Comparative In Vitro and In Vivo Quantifications of Pathologic Tau Deposits and Their Association with Neurodegeneration in Tauopathy Mouse Models. *J. Nucl. Med.* **2018**, *59*, 960–966.

(35) Leuzy, A.; Chiotis, K.; Lemoine, L.; Gillberg, P.-G.; Almkvist, O.; Rodriguez-Vieitez, E.; Nordberg, A. Tau PET imaging in neurodegenerative tauopathies—still a challenge. *Mol. Psychiatry* **2019**, *24*, 1112–1134.

(36) Walji, A. M.; Hostetler, E. D.; Selnick, H.; Zeng, Z.; Miller, P.; Bennacef, I.; Salinas, C.; Connolly, B.; Gantert, L.; Holahan, M.; O'Malley, S.; Purcell, M.; Riffel, K.; Li, J.; Balsells, J.; O'Brien, J. A.; Melquist, S.; Soriano, A.; Zhang, X.; Ogawa, A.; Xu, S.; Joshi, E.; Della Rocca, J.; Hess, F. J.; Schachter, J.; Hesk, D.; Schenk, D.; Struyk, A.; Babaoglu, K.; Lohith, T. G.; Wang, Y.; Yang, K.; Fu, J.; Evelhoch, J. L.; Coleman, P. J. Discovery of 6-(Fluoro-(18)F)-3-(1H-pyrrolo[2,3-c]pyridin-1-yl)isoquinolin-5-amine ([18F]-MK-6240): A Positron Emission Tomography (PET) Imaging Agent for Quantification of Neurofibrillary Tangles (NFTs). *J. Med. Chem.* **2016**, *59*, 4778–4789.

(37) Lohith, T. G.; Bennacef, I.; Vandenberghe, R.; Vandenberghe, M.; Salinas, C.; Declercq, R.; Reyniers, T.; Telan-Choing, F.; Riffel, K.; Celen, S.; Serdons, K.; Bormans, G.; Tsai, K.; Walji, A.; Hostetler, E. D.; Evelhoch, J. L.; Van Laere, K.; Forman, M.; Stoch, A.; Sur, C.; Struyk, A. Brain Imaging of Alzheimer Dementia Patients and Elderly Controls with ¹⁸F-MK-6240, a PET Tracer Targeting Neurofibrillary Tangles. *J. Nucl. Med.* **2019**, *60*, 107–114.

(38) Rombouts, F. J.; Andres, J. I.; Ariza, M.; Alonso, J. M.; Austin, N.; Bottelbergs, A.; Chen, L.; Chupakhin, V.; Cleiren, E.; Fierens, K.; Fontana, A.; Langlois, X.; Leenaerts, J. E.; Marien, J.; Martinez Lamencia, C.; Salter, R.; Schmidt, M. E.; Te Riele, P.; Wintmolders, C.; Trabanco, A. A.; Zhang, W.; Macdonald, G.; Moechars, D. Discovery of N-(Pyridin-4-yl)-1,5-naphthylidene-2-amine as Potential Tau Pathology PET Tracers for Alzheimer's Disease. *J. Med. Chem.* **2017**, *60*, 1272–1291.

(39) Rombouts, F. J. R.; Declercq, L.; Andrés, J.-I.; Bottelbergs, A.; Chen, L.; Iturrino, L.; Leenaerts, J. E.; Mariën, J.; Song, F.; Wintmolders, C.; Wuyts, S.; Xia, C. A.; te Riele, P.; Bormans, G.; Vandenberghe, R.; Kolb, H.; Moechars, D. Discovery of N-(4-[18F]Fluoro-5-methylpyridin-2-yl)isoquinolin-6-amine (JNJ-64326067), a New Promising Tau Positron Emission Tomography Imaging Tracer. *J. Med. Chem.* **2019**, *62*, 2974–2987.

(40) Kolb, H. C.; Moechars, D.; Rombouts, F.; Schmidt, M. E.; Szardenings, A. K.; Timmers, M.; Barret, O.; Madonia, J.; Marek, K.; Sandiego, C. Imaging Alzheimer's Tau Pathology In Humans: [18f]JNJ-067 A Phase 0 Exploratory Study In Healthy Volunteers And Subjects With Probable Alzheimer's Disease. *Alzheimer's Dementia* **2018**, *14*, P838.

(41) Gobbi, L. C.; Knust, H.; Korner, M.; Honer, M.; Czech, C.; Belli, S.; Muri, D.; Edelmann, M. R.; Hartung, T.; Erbsmehl, I.; Grall-Ulsemmer, S.; Koblet, A.; Rueher, M.; Steiner, S.; Ravert, H. T.; Mathews, W. B.; Holt, D. P.; Kuwabara, H.; Valentine, H.; Dannals, R. F.; Wong, D. F.; Borroni, E. Identification of Three Novel Radiotracers for Imaging Aggregated Tau in Alzheimer's Disease with Positron Emission Tomography. *J. Med. Chem.* **2017**, *60*, 7350–7370.

(42) Wong, D. F.; Comley, R.; Kuwabara, H.; Rosenberg, P. B.; Resnick, S. M.; Ostrowitzki, S.; Vozzi, C.; Boess, F.; Oh, E.; Lyketsos, C. G.; Honer, M.; Gobbi, L.; Klein, G.; George, N.; Gaspas, L.; Kitzmiller, K.; Roberts, J.; Sevigny, J.; Nandi, A.; Brasic, J. R.; Mishra, C.; Thambisetty, M.; Moghekar, A.; Mathur, A.; Albert, M.; Dannals, R. F.; Borroni, E. Characterization of 3 Novel Tau Radiopharmaceuticals, ¹¹C-RO-963, ¹¹C-RO-643, and ¹⁸F-RO-948, in Healthy Controls and in Alzheimer Subjects. *J. Nucl. Med.* **2018**, *59*, 1869–1876.

- (43) Rejc, L.; Smid, L.; Kepe, V.; Podlipnik, C.; Golobic, A.; Bresjanac, M.; Barrio, J. R.; Petric, A.; Kosmrlj, J. Design, Syntheses, and in Vitro Evaluation of New Fluorine-18 Radiolabeled Tau-Labeling Molecular Probes. *J. Med. Chem.* **2017**, *60*, 8741–8757.
- (44) Kroth, H.; Oden, F.; Molette, J.; Schieferstein, H.; Capotosti, F.; Mueller, A.; Berndt, M.; Schmitt-Willich, H.; Darmency, V.; Gabellieri, E.; Boudou, C.; Juergens, T.; Varisco, Y.; Vokali, E.; Hickman, D. T.; Tamagnan, G.; Pfeifer, A.; Dinkelborg, L.; Muhs, A.; Stephens, A. Discovery and preclinical characterization of [¹⁸F]PI-2620, a next-generation tau PET tracer for the assessment of tau pathology in Alzheimer's disease and other tauopathies. *Eur. J. Nucl. Med. Mol. Imaging* **2019**, *46*, 2178–2189.
- (45) Mueller, A.; Bullich, S.; Barret, O.; Madonia, J.; Berndt, M.; Papin, C.; Perrotin, A.; Koglin, N.; Kroth, H.; Pfeifer, A.; Tamagnan, G.; Seibyl, J. P.; Marek, K.; De Santi, S.; Dinkelborg, L. M.; Stephens, A. W. Tau PET imaging with ¹⁸F-PI-2620 in Patients with Alzheimer Disease and Healthy Controls: A First-in-Humans Study. *J. Nucl. Med.* **2020**, *61*, 911–919.
- (46) Sanabria Bohórquez, S.; Marik, J.; Ogasawara, A.; Tinianow, J. N.; Gill, H. S.; Barret, O.; Tamagnan, G.; Alagille, D.; Ayalon, G.; Manser, P.; Bengtsson, T.; Ward, M.; Williams, S.-P.; Kerchner, G. A.; Seibyl, J. P.; Marek, K.; Weimer, R. M. [¹⁸F]GTP1 (Genentech Tau Probe 1), a radioligand for detecting neurofibrillary tangle tau pathology in Alzheimer's disease. *Eur. J. Nucl. Med. Mol. Imaging* **2019**, *46*, 2077–2089.
- (47) Cui, M.; Ono, M.; Kimura, H.; Liu, B.; Saji, H. Novel quinoxaline derivatives for in vivo imaging of beta-amyloid plaques in the brain. *Bioorg. Med. Chem. Lett.* **2011**, *21*, 4193–4196.
- (48) Yoshimura, M.; Ono, M.; Matsumura, K.; Watanabe, H.; Kimura, H.; Cui, M.; Nakamoto, Y.; Togashi, K.; Okamoto, Y.; Ihara, M.; Takahashi, R.; Saji, H. Structure-Activity Relationships and in Vivo Evaluation of Quinoxaline Derivatives for PET Imaging of beta-Amyloid Plaques. *ACS Med. Chem. Lett.* **2013**, *4*, 596–600.
- (49) Yu, P.; Cui, M.; Wang, X.; Zhang, X.; Li, Z.; Yang, Y.; Jia, J.; Zhang, J.; Ono, M.; Saji, H.; Jia, H.; Liu, B. ¹⁸F-labeled 2-phenylquinoxaline derivatives as potential positron emission tomography probes for in vivo imaging of beta-amyloid plaques. *Eur. J. Med. Chem.* **2012**, *57*, 51–58.
- (50) Fu, H. L.; Cui, M. C.; Zhao, L.; Tu, P. Y.; Zhou, K. X.; Dai, J. P.; Liu, B. L. Highly Sensitive Near-Infrared Fluorophores for in Vivo Detection of Amyloid-beta Plaques in Alzheimer's Disease. *J. Med. Chem.* **2015**, *58*, 6972–6983.
- (51) Barghorn, S.; Davies, P.; Mandelkow, E. Tau paired helical filaments from Alzheimer's disease brain and assembled in vitro are based on beta-structure in the core domain. *Biochemistry* **2004**, *43*, 1694–1703.
- (52) Crowe, A.; Ballatore, C.; Hyde, E.; Trojanowski, J. Q.; Lee, V. M. Y. High throughput screening for small molecule inhibitors of heparin-induced tau fibril formation. *Biochem. Biophys. Res. Commun.* **2007**, *358*, 1–6.
- (53) Cai, L.; Qu, B.; Hurtle, B. T.; Dadiboyena, S.; Diaz-Arrastia, R.; Pike, V. W. Candidate PET Radioligand Development for Neurofibrillary Tangles: Two Distinct Radioligand Binding Sites Identified in Postmortem Alzheimer's Disease Brain. *ACS Chem. Neurosci.* **2016**, *7*, 897–911.
- (54) Naslund, J.; Haroutunian, V.; Mohs, R.; Davis, K. L.; Davies, P.; Greengard, P.; Buxbaum, J. D. Correlation between elevated levels of amyloid beta-peptide in the brain and cognitive decline. *JAMA* **2000**, *283*, 1571–1577.
- (55) Mukaetova-Ladinska, E. B.; Harrington, C. R.; Roth, M.; Wischik, C. M. Biochemical and anatomical redistribution of tau protein in Alzheimer's disease. *Am. J. Pathol.* **1993**, *143*, 565–578.
- (56) Yang, Y.; Wang, X.; Yang, H.; Fu, H.; Zhang, J.; Zhang, X.; Dai, J.; Zhang, Z.; Lin, C.; Guo, Y.; Cui, M. Synthesis and Monkey-PET Study of (R)- and (S)-¹⁸F-Labeled 2-Arylbenzoheterocyclic Derivatives as Amyloid Probes with Distinctive in Vivo Kinetics. *Mol. Pharmaceutics* **2016**, *13*, 3852–3863.
- (57) Ng, K. P.; Pascoal, T. A.; Mathotaarachchi, S.; Therriault, J.; Kang, M. S.; Shin, M.; Guiot, M.-C.; Guo, Q.; Harada, R.; Comley, R. A.; Massarweh, G.; Soucy, J.-P.; Okamura, N.; Gauthier, S.; Rosa-Neto, P. Monoamine oxidase B inhibitor, selegiline, reduces 18F-THK5351 uptake in the human brain. *Alzheimer's Res. Ther.* **2017**, *9*, 25.
- (58) Santana, L.; González-Díaz, H.; Quezada, E.; Uriarte, E.; Yáñez, M.; Viña, D.; Orallo, F. Quantitative Structure-Activity Relationship and Complex Network Approach to Monoamine Oxidase A and B Inhibitors. *J. Med. Chem.* **2008**, *51*, 6740–6751.
- (59) Yung-Chi, C.; Prusoff, W. H. Relationship between the inhibition constant (K_i) and the concentration of inhibitor which causes 50% inhibition (I_{50}) of an enzymatic reaction. *Biochem. Pharmacol.* **1973**, *22*, 3099–3108.